Available online at www.sciencedirect.com

ScienceDirect

Underground Space 27 (2026) 24–44

www.keaipublishing.com/undsp

Research Paper

Effects of shield tunnelling parameters on the long-term settlement of piled buildings in soft ground

Ruikun Wang [a,b], Gang Zheng [a,b], Huayang Lei [a,b], Xuesong Cheng [a,b,*], Eng-Choon Leong [c], Yetao Ji [d]

[a] *MOE Key Laboratory of Coast Civil Structure Safety, Tianjin University, Tianjin 300072, China*
[b] *Department of Civil Engineering, Tianjin University, Tianjin 300072, China*
[c] *School of Civil & Environmental Engineering, Nanyang Technological University, Singapore 639798, Singapore*
[d] *China Railway Tunnel Group Road & Bridge Engineering Co., Ltd., Tianjin 300308, China*

Received 1 April 2025; received in revised form 26 September 2025; accepted 28 October 2025
Available online 5 January 2026

Abstract

This study investigated the long-term settlement behaviour of piled buildings induced by shield tunnelling in soft ground conditions within urban environments. By integrating a detailed case study with advanced numerical modelling techniques, this study provided a nuanced understanding of the interactions between tunnel construction and existing pile foundations. Central to the investigation is the role of soil consolidation, which significantly contributes to the settlement of piled buildings. To address this, this study emphasizes the critical need for the precise calibration of tunnelling parameters such as face pressure and grouting pressures. These parameters are meticulously controlled to mitigate the adverse effects on nearby piled buildings, ensuring their stability and integrity. It is established that an optimal face pressure, set at 90% of the lateral earth pressure, consistently minimizes the settlement of piled buildings, primarily due to the minimal reduction in the pile toe resistance observed near the tunnel. Similarly, the ideal grouting pressure was identified to be within the range of 120%–160% of the vertical earth pressure, with the smallest building settlement and decrease in pile toe resistance observed at a grouting pressure of 150% of the overburden pressure. This finding elucidates the load transfer mechanism within piled buildings. This study further demonstrated that the settlement induced by the second tunnel excavation is smaller than that caused by the first tunnel excavation owing to the sheltering effects of the adjacent first tunnel and pile foundations. During the consolidation phase following tunnel excavation, the settlement caused by the second tunnel is smaller than that caused by the first tunnel, which is attributed to the dissipation of the negative excess pore pressure around the first tunnel, leading to soil volume expansion. These insights not only validate the effectiveness of the numerical model but also contribute significantly to the field of geotechnical engineering by providing actionable guidelines for future tunnelling projects.

Keywords: Long-term settlement behaviour; Tunnelling parameters; Load transfer mechanism; Piled building

1 Introduction

High-rise buildings have become a hallmark of economic growth and architectural advancement across cities worldwide. Deep foundation systems, such as pile groups and piled raft foundations, are increasingly employed to ensure sufficient bearing capacity and to maintain the structural integrity of these towering edifices (Chore et al., 2010; Józefiak et al., 2015; Randolph, 2003). Meanwhile, the surge in demand for sustainable transport infrastructure, driven by rapid urbanization, has necessitated the construction of numerous tunnels in recent years.

Managing the settlement of piled buildings induced by tunnelling in both short-term and long-term conditions is of paramount concern. The short-term settlement occurs

* Corresponding author at: MOE Key Laboratory of Coast Civil Structure Safety, Tianjin University, Tianjin 300072, China.
E-mail address: xuesong.cheng@tju.edu.cn (X. Cheng).
Peer review under the responsibility of Tongji University

https://doi.org/10.1016/j.undsp.2025.10.003

during the construction phase, chiefly as a direct reaction of the soil to excavation activities, and is characterized by both vertical and horizontal movements. Conversely, long-term settlement progressively evolves over time, driven by factors such as soil consolidation, with soft clay being particularly susceptible. This susceptibility is well-documented in studies by Komiya et al. (2006), Shirlaw (1995), Ng et al. (2013a), and Meng et al. (2018), which highlight the ongoing nature of settlement in soft clay layers. A notable instance of this phenomenon was examined by Boonyarak et al. (2014), who studied a tunnel constructed adjacent to an expressway pier utilizing the earth pressure balance shield in stiff clay conditions. Throughout and after the tunnel excavation, the settlement and inclination of the piers were meticulously monitored. Observations showed that long-term settlement often results from the dissipation of excess pore water pressure within the soft soil surrounding tunnels, accounting for approximately 80% of the total settlement.

In shield tunnelling, the stability and safety of the structure are of paramount importance, predominantly influenced by critical tunnelling parameters such as face and grouting pressures. Liu (2014) conducted an investigation into the response of an adjacent pile group to large-diameter tunnelling. The entire process of tunnelling adjacent to the pile foundation was accurately replicated using numerical modelling, taking into consideration factors such as the face pressure, grouting pressure, and the interaction between the piles and soil. Furthermore, Jeon et al. (2020) demonstrated that the face pressure significantly influences the settlement behavior of piled buildings. The findings revealed that with decreasing face pressure, there was a marked increase in surface settlements, pile head settlements, axial pile forces, and shear stress at the pile–soil interface. The control of the settlement of piled buildings, a crucial aspect of tunnel construction, has been extensively studied. The aforementioned studies emphasize the significance of selecting optimal tunnelling parameters during shield tunnelling. Various approaches have been employed to comprehend and mitigate the adverse effects of tunnelling on the surrounding environment, thereby ensuring the structural integrity and longevity of both the tunnel and adjacent infrastructures. However, the impact of critical tunnelling parameters on long-term settlement remains underexplored, yet not explained in the studies by Liu (2014) and Jeon et al. (2020). The implications of such critical tunnelling parameters on the long-term settlement of piled buildings necessitate a deeper understanding, given their direct influence on the longevity and functionality of the tunnel and surrounding infrastructure, especially within regions characterized by soft soil.

Many studies have conducted comprehensive analyses that encapsulate the complex interactions among the soil, tunnel, and pile foundation systems. A wealth of knowledge has been obtained through field observations (Pang, 2006; Selemetas, 2006; Selemetas & Standing, 2018), theoretical analyses (Cao et al., 2023; Gokuldas et al., 2020; Huang et al., 2022; Marshall, 2012; Sun et al., 2024), numerical simulations (Cheng et al., 2007; Hong et al., 2015a, 2015b; Jongpradist et al., 2013; Lee, 2012; Soomro, 2021; Soomro et al., 2015, 2017, 2018, 2020, 2022), and model tests (Chen et al., 2018; Franza & Marshall, 2018; Lu et al., 2020; Ng et al., 2013b, 2015). These studies conducted extensive analyses concerning the complex interactions of the soil, tunnel, and pile foundations during shield tunnelling. Cheng et al. (2007) used two-dimensional finite element models to simplify the analysis of tunnel–pile interactions. These models simplified the tunnelling process by applying uniform volume loss and contraction-based methods to simulate ground loss, neglecting the detailed construction sequence, which limited their ability to capture the three-dimensional nature of soil displacement and pile–soil–tunnel interactions. Lee (2012) utilized a three-dimensional finite element model but relied on the Mohr–Coulomb soil model, which often underestimates the shear stress transfer at pile–soil interfaces due to its simplified constitutive behavior. Notably, earlier studies predominantly focused on axial pile forces and lateral pile displacements induced by tunnelling, yet rarely conducted a thorough analysis of the load transfer mechanisms at the pile–soil interface, which are critical to understanding pile behavior. Lu et al. (2020) demonstrated that tunnelling at varying depths significantly altered the load distribution on piles, with tunnels near the pile toe reducing the load by 22% and those adjacent to the pile shaft increasing the load by 21.7%. Soomro et al. (2015, 2017, 2018, 2020, 2022) further investigated the response of pile groups to multitrack tunnelling, considering diverse pile configurations relative to twin tunnels. Their studies integrated three-dimensional numerical simulations with centrifuge model tests to elucidate the load transfer mechanisms influenced by the spatial relationship between tunnels and pile groups, offering a more comprehensive understanding of these interactions. However, most previous studies focused on immediate excavation-induced settlements, with limited attention paid to the long-term consolidation effects in soft soil. This gap is significant for soft soil, where consolidation contributes significantly to the total settlement.

This paper introduces a shield tunnelling project that elucidated critical aspects such as line alignment, hydrogeology, and the positioning of the tunnel relative to an adjacent piled building. Subsequently, the research focuses on monitoring the response of the piled building to shield tunnelling activities. To achieve a high accuracy in replicating the tunnel construction process, a three-dimensional soil–fluid coupled numerical model was developed. The reliability of this numerical model was subsequently validated through a rigorous comparison between computed and measured data, ensuring the model's efficacy in simulating practical tunnelling impacts. The primary objective of this study was to analyse and interpret the impacts of critical tunnelling parameters, including face and grouting pressures, on the long-term settlement of piled buildings

induced by shield tunnelling. Various load transfer mechanisms after tunnel construction were considered in these analyses, aiming to provide a comprehensive understanding of their impact on tunnel stability and adjacent infrastructure. This holistic approach aimed to elucidate the complex dynamics between tunnelling and the resultant structural responses, thereby contributing to the optimization of tunnel design and construction practices.

2 Project profile

2.1 Overview of shield tunnelling under high-risk piled buildings

As shown in Fig. 1, the proposed scheme for the Northern Section of Line 4 of the Tianjin Metro crosses the most congested central urban area and the urban–rural fringe of Tianjin, stretching from Xiaojie Station in Beichen District in the north to Hebei Street Station in Hongqiao District in the south. The main line has a total length of approximately 21.95 km and comprises 17 stations. This project consists of two parallel tunnels, with the excavation of the left tunnel initiated after the commencement of the right tunnel. An earth pressure balance shield machine (EPBM), measuring 8.7 m in length and 6.4 m in diameter, is utilized for the excavation.

The relative positional relationship between the shield tunnel of Line 4 and the high-risk buildings is illustrated in Fig. 2. The tunnel cover depth is 21.7 to 31.8 m. The pile lengths of the piled buildings vary from 15.5 to 30 m, with the distances from the tunnel crown to pile toe ranging from 0.77 to 5.80 m. The spacing between the parallel twin tunnels is between 10.4 and 18.2 m, whereas the distance from the *O*-point to the centreline of the buildings ranges from 0 to 12.7 m. The *O*-point represents the geometric centre of the parallel twin tunnels. This indicates that the tunnel unavoidably passes adjacent to piled buildings during construction, and the spatial proximity between the tunnel and piled buildings becomes even tighter when the distance from the *O*-point to the building centreline is smaller, thereby increasing the construction difficulty and risk significantly.

The shield tunnel passed beneath a piled building during construction, a process that inherently influences such structures. Tunnel excavations can introduce significant construction risks and potential safety hazards to piled buildings. For safety considerations, a transverse monitoring section was designated to systematically monitor the impact of tunnelling. Various instruments were installed at this section to observe the long-term settlements of the surface and adjacent piled buildings. These observations commenced with the onset of tunnel excavation and continued until 180 days after the completion of the twin tunnels, as illustrated in Fig. 2.

Figure 2 illustrates the soil profile at the monitoring section, indicating that the soil layers primarily consist of silty clay and sandy silt. The groundwater regime at this location is characterized as hydrostatic, with the water table situated approximately at the ground level. Table 1 presents a detailed summary of the critical geotechnical parameters for each soil layer in the profile. The excavation undertaken by the shield machine primarily progresses through silty clay strata. Each tunnel lining segment has an outer diameter of 6.2 m, a width of 1.5 m, and a thickness of 0.35 m.

Fig. 1. Plan view of the tunnelling project.

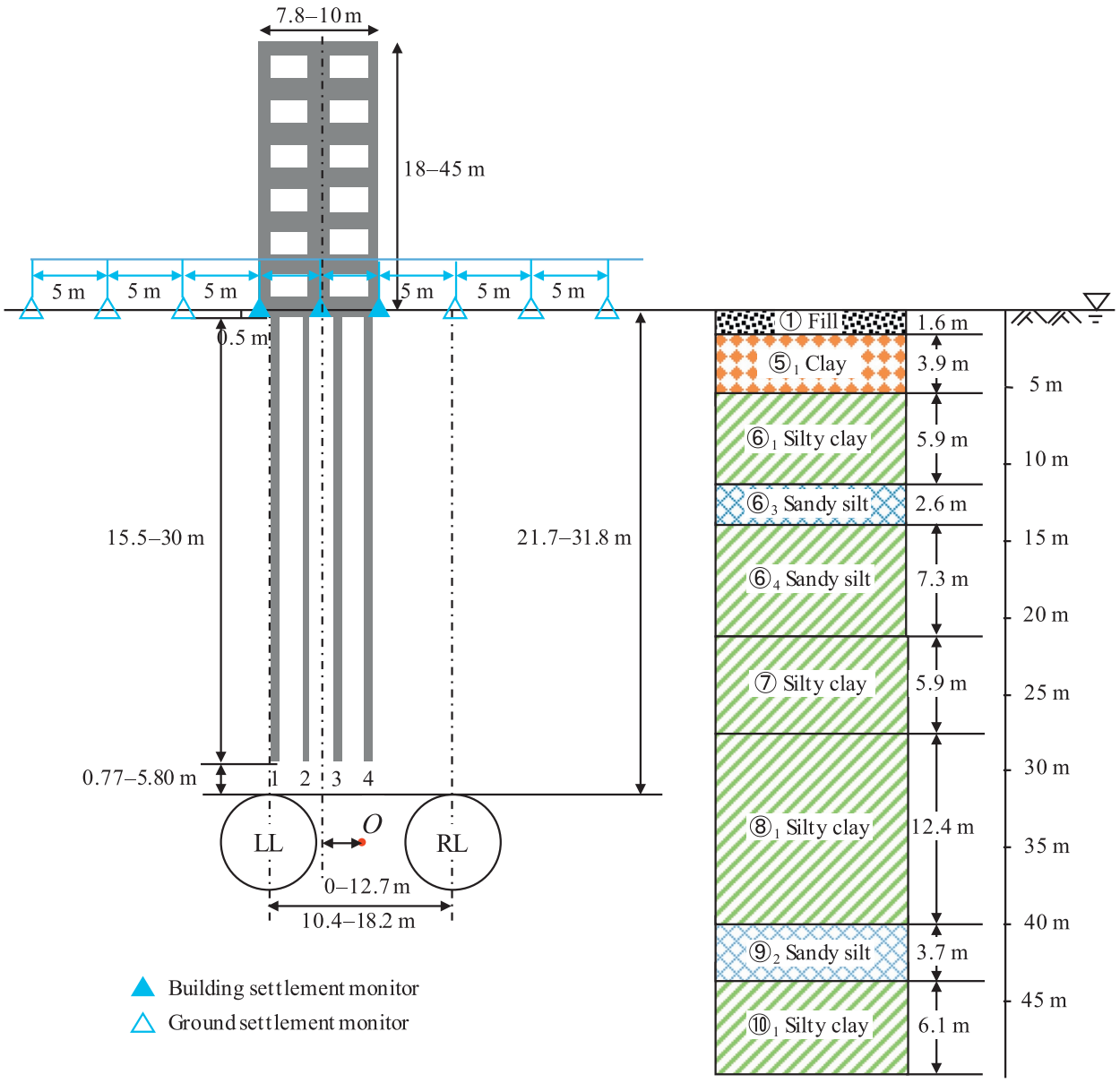

Fig. 2. Monitoring section diagram illustrating the relative relationship between the pile-foundation buildings and twin tunnels.

Table 1
Geotechnical parameters of the soil strata.

Soil layer	Unit weight (kN/m^3)	λ	κ	M	e_o	Permeability coefficient (m/d)
①$_1$ Fill	18.2	0.067	0.0084	0.57	0.84	5.0×10^{-1}
⑤$_1$ Clay	18.69	0.089	0.0097	1.01	0.70	5.93×10^{-3}
⑥$_1$ Silty clay	19.78	0.059	0.0073	1.10	0.82	2.37×10^{-3}
⑥$_3$ Sandy silt	20.43	0.026	0.0031	1.48	0.47	1.85×10^{-1}
⑥$_4$ Silty clay	19.49	0.046	0.0053	1.05	0.69	1.52×10^{-3}
⑦ Silty clay	18.93	0.070	0.0074	0.84	0.63	1.18×10^{-1}
⑧$_1$ Silty clay	19.54	0.085	0.0156	0.73	0.79	3.39×10^{-4}
⑨$_2$ Sandy silt	20.98	0.016	0.0025	1.46	0.66	1.28×10^{-1}
⑩$_1$ Silty clay	20.84	0.058	0.0094	1.11	0.65	1.05×10^{-4}

2.2 Measured settlements of piled buildings

Figure 3 illustrates the measured settlements of the piled buildings at the monitoring section. Two shield tunnel construction cases were selected, where the tunnels were in proximity to the overlying existing piled buildings.

Case 1: The pile length is 16.5 m, with a cover depth of 21.7 m at the tunnel crown. The distance between the

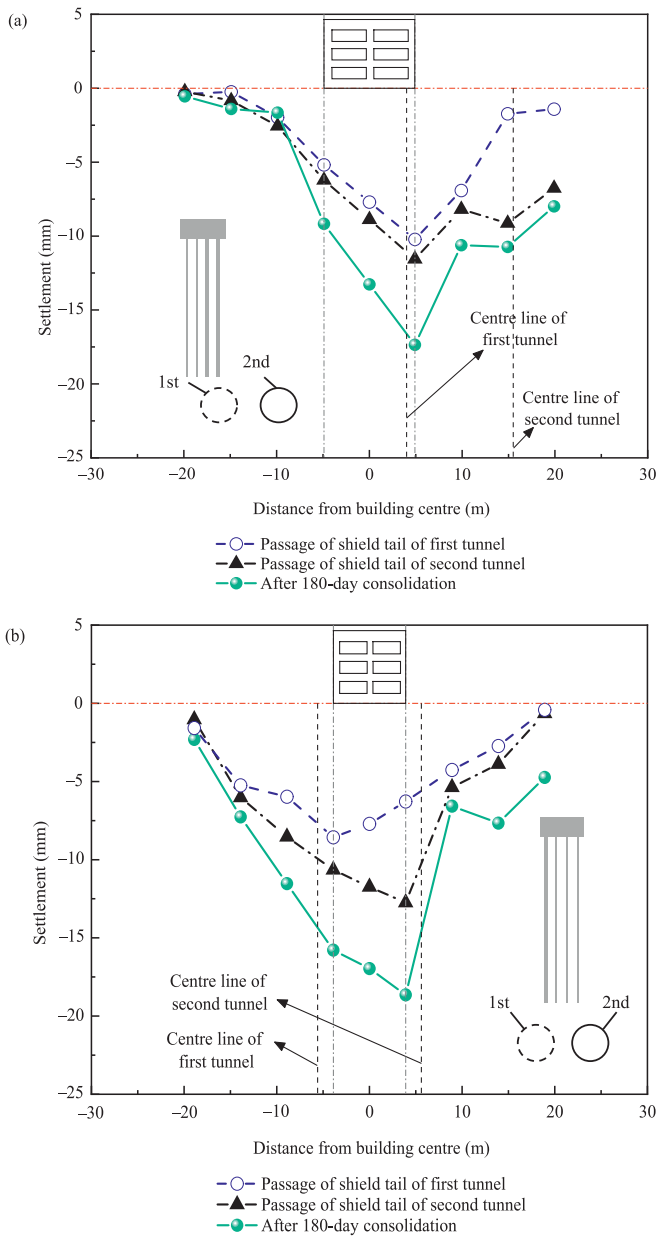

Fig. 3. Measured settlements of piled buildings. (a) Case 1, and (b) Case 2.

tunnel crown and pile toe is 5.2 m. The twin tunnels were excavated in a parallel arrangement with a centre-to-centre spacing of 10.6 m between the two tunnels. The piled building consists of six stories, measuring 21.5 m in length, 10.4 m in width, and 18 m in height. Each storey has a height of 3 m. The building is supported by a pile foundation, comprising a total of 40 piles (arranged in a 4 × 10 group). The settlement of the building caused by the shield construction is illustrated in Fig. 3(a).

Case 2: The pile length is 31.5 m, with a cover depth of 21.7 m at the tunnel crown. The distance between the tunnel crown and the pile toe is 2.0 m. The parallel twin tunnels have a centre-to-centre spacing of 11.2 m. The high-rise building consists of 15 stories, with dimensions of 19.5 m in length, 7.8 m in width, and 45 m in height, with each storey having a height of 3 m. The building spans two bays in width and five bays in length. It is supported by a pile foundation, comprising a total of 40 piles arranged in a 4 × 10 group. The settlement of the building caused by shield construction is shown in Fig. 3(b).

As shown in Fig. 3, the building settlements generally exceed those of the surrounding soil settlements. For Case 1, after the shield tail passed, the maximum building settlement was 8.09 mm, and the differential settlement was 3.74 mm. After the completion of shield construction and subsequent soil consolidation, the maximum building settlement increased to 12.15 mm, and the differential settlement increased to 6.42 mm. This indicates that soil consolidation not only increases soil settlement but also contributes to an increase in building settlement and inclination.

For Case 2, because both tunnels pass beneath the piled building and the distance between the tunnel crown and building is small, the maximum building settlement after the shield tail passed was 12.74 mm, with a differential settlement of 2.10 mm. During the soil consolidation phase, the maximum building settlement increased further to 18.64 mm, and the differential settlement increased to 2.86 mm, with the consolidation settlement accounting for approximately 32% of the total settlement. This demonstrated that during the soil consolidation phase, building settlements significantly increase, and the consolidation effect has a considerable impact on the long-term settlement. Therefore, controlling construction-induced and secondary consolidation settlements during the consolidation phase is critical to ensuring the safety of piled buildings.

3 Establishment and validation of the numerical model

3.1 Establishment of the numerical model

To investigate the soil response to tunnelling, a soil–tunnel coupled numerical model was established based on the abovementioned project. Numerical analyses were carried out utilizing the soil–fluid coupled three-dimensional finite element method, employing the commercial finite element software ABAQUS (version 2020). The simulation focused on the shield tunnelling in Case 2, involving a high-rise piled building.

The model was designed to simulate the shield tunnelling process in soft ground conditions, specifically focusing on the interactions among the tunnel, surrounding soil, and adjacent pile foundations. The simulation targeted Case 2, which involved a 15-storey high-rise building supported by a pile foundation.

3.1.1 Mesh and boundary conditions

Figure 4 shows the finite element mesh utilized in this study. The model incorporated eight-node hexahedral solid elements (C3D8P) to simulate both the soil and grout and quadrilateral shell elements (S4) for the shield and tunnel lining. The model was 80 m high and 120 m wide. The lateral boundaries were positioned at a distance of 8*D*

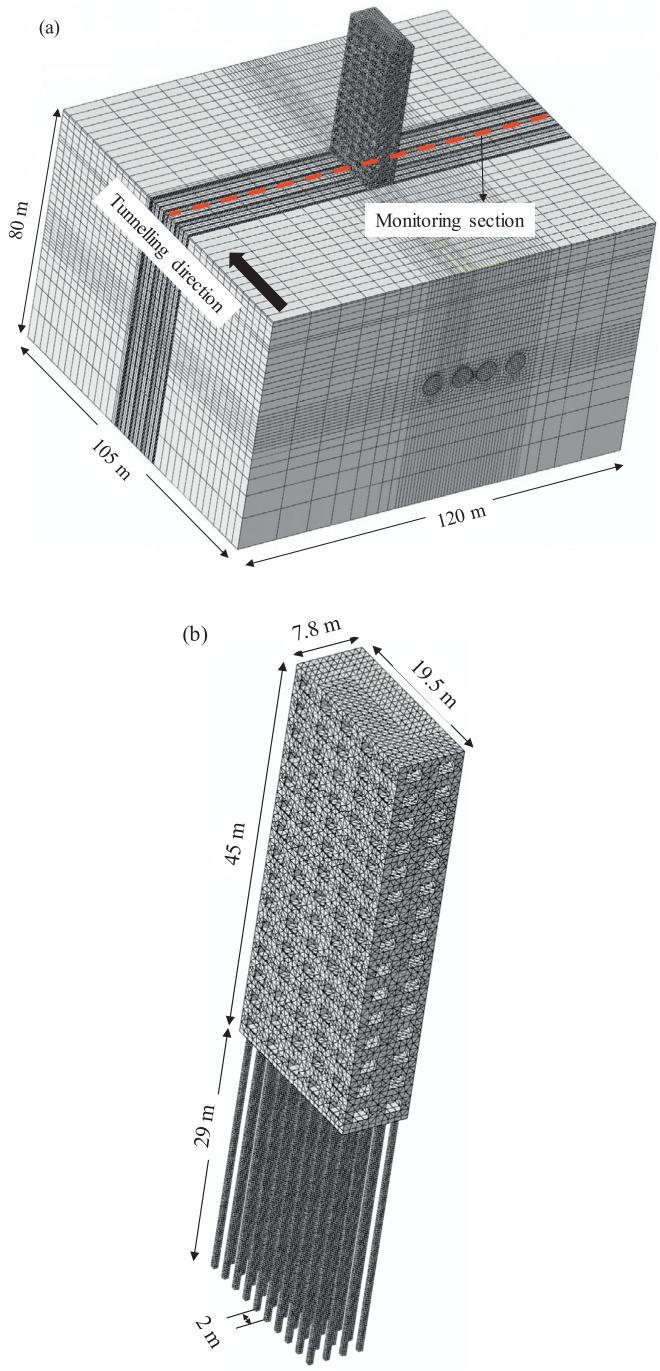

Fig. 4. Schematic of 3D FE mesh employed in the tunnelling simulation. (a) Tunnelling beneath a piled building, and (b) model of the piled building.

(D represents the outer diameter of tunnel lining) from the tunnel axis to minimize the influence of the boundary conditions on the results (Franzius & Potts, 2005). The longitudinal length of the model was set to 105 m, accommodating the total length of 70 lining rings.

Vertical displacements were constrained at the bottom boundary, whereas the lateral boundaries were restricted in the normal direction. Based on a geotechnical exploration report, the groundwater table was set at the ground surface with a fixed pore pressure of zero to reflect the hydrostatic groundwater regime observed at the site. The pore pressure boundary conditions on both lateral sides of the model were configured to increase linearly with depth, following a triangular distribution to represent the natural hydrostatic pressure gradient. The top surface of the model was set to allow drainage, simulating free-draining conditions at the ground surface. To account for tunnel waterproofing requirements, the model adhered to Technical code for waterproofing of underground works, which mandates that the average seepage volume should not exceed 0.05 L/(m^2·d). Tunnel leakage was modeled by specifying the seepage velocity directly on the tunnel surface using the "surface pore fluid" load option in ABAQUS (Jin et al., 2022). This approach simulated the comprehensive peripheral penetration of the tunnel and captured the limited seepage allowed under the specified waterproofing standards.

The modified cam-clay (MCC) model was employed in the numerical simulation of tunnelling in soft ground in Tianjin (Zheng et al., 2015a, 2022). In the simulation, the soil stratus was normally consolidated, with an optical character recognition of 1 for fine-grained layers. The derivations of critical soil parameters essential for this model are detailed in the abovementioned papers.

3.1.2 Model of piled building

Figure 4 shows a 15-storey masonry–concrete structure supported by a pile foundation. Each storey of the building is 3 m high, resulting in a building height of 45 m. The dimensions of the piled building are 7.8 m in width and 19.5 m in length. The structural thicknesses of the walls and floors are 0.30 and 0.18 m, respectively. The raft associated with the building has a thickness and cover depth of 0.5 m each. A 4 × 10 pile group is located beneath the raft. The width and length of each reinforced concrete square pile are 0.48 and 29 m, respectively. The pile spacing is 2 m. The detailed parameters of these components are tabulated in Table 2.

As depicted in Fig. 4(b), the simulation employed a triangular shell element (S3) to model the walls and floors of the building, whereas 8-node hexahedral solid elements (C3D8R) were adopted for the raft and pile foundations. Moreover, the building was rigidly connected to a reinforced concrete raft. Meanwhile, the interaction between the piles and the surrounding soil was modeled using the

Table 2
Parameters of building components.

Material	Young's modulus (GPa)	Unit weight (kN/m^3)	Poisson's ratio
Floor	30	25	0.2
Wall	6	20	0.2
Raft foundation	30	25	0.2
Pile	30	25	0.2

surface-to-surface contact option in ABAQUS. The normal behaviour of the contact was set as hard contact with no normal relative displacement. The tangential behavior was set as Coulomb friction, in which the friction coefficient and finite sliding distance were required as input parameters. The friction coefficient and finite sliding distance were 0.3 and 5 mm, respectively (Zheng et al., 2023). This approach accounted for the frictional and normal forces at the pile–soil interface, enabling a realistic simulation of the shear stress and load transfer between the pile and soil.

3.1.3 Modelling procedure

Figure 5 illustrates the modeling procedure for the shield tunnelling. The construction of the tunnel was divided into several steps, each described as a sequence of operations according to Zheng et al. (2015a).

(1) Soil excavation: Soil elements ahead of the tunnel face were removed to simulate the excavation process. A completely impermeable boundary was established at the tunnel face to prevent the fluid flow through the excavation surface.
(2) Shield update: After soil excavation, the shield model was advanced by one tunnel ring length (1.5 m), reflecting the incremental progression of the EPBM.
(3) Forces application: Face pressure P_f was applied to a freshly exposed tunnel face. The pressure was set according to the lateral earth pressure observed at the cover depth. P_f was configured to increase linearly with the depth at a gradient of 10 kN/m^2/m. Furthermore, a hydraulic jack force F_j was applied to the shield. Based on engineering practice, F_j typically represents 40% to 60% of the total thrust. In this model, F_j was set to 50% of the total thrust, which was equivalent to the resultant force of P_f.
(4) Lining and shield tail grouting: A lining ring measuring 1.5 m was installed behind the shield tail as the shield advanced. Considering the resistance encountered during the grout injection from the pipelines, the actual pressure exerted on the soil mass was lower than the recorded pressure. Therefore, a reduction of 80 kPa was applied to the grouting pressure in the numerical simulation according to Zheng et al. (2015b). P_g was assumed to increase linearly with depth at a gradient of 10 kPa/m. The lining and grout parameters were exhaustively explained by Zheng et al. (2022). Hence, further details are not provided in this paper.

After the excavation of both tunnels, a 180-day consolidation period was simulated to compare the computed and measured surface settlements owing to soil consolidation. For parametric studies, a longer 10-year consolidation period was applied to assess the long-term settlement behavior.

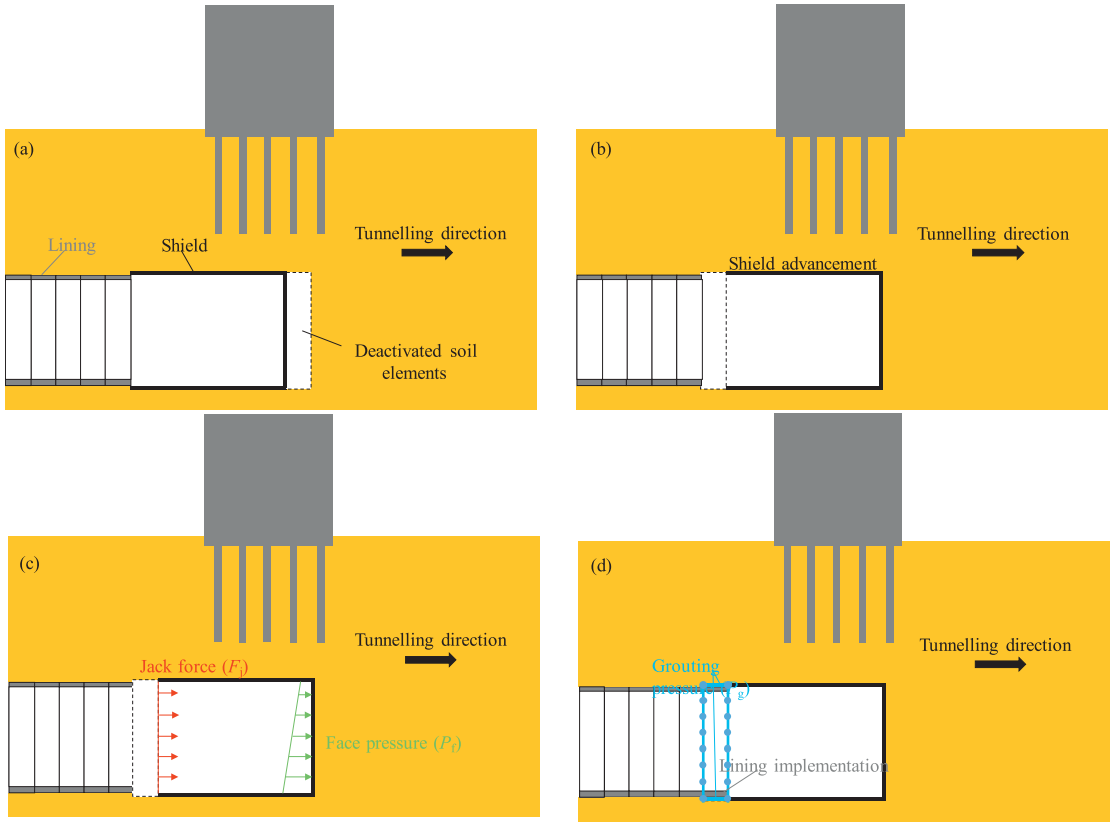

Fig. 5. Schematic of shield tunnelling. (a) Soil excavation, (b) shield update, (c) forces application, and (d) lining and shield tail grouting. (Zheng et al., 2022)

3.2 Comparisons of the measured and computed data

Figure 6(a) illustrates the time history of the maximum settlements of the piled building. This indicated that the settlement induced during the excavation of the second tunnel was smaller than that during the excavation of the first tunnel. Figure 6(b) illustrates the computed and measured settlements of the surface and piled building at the monitoring section. The computed maximum building settlement induced by the first tunnel (LL) was 7.6 mm, which was closely aligned with the measured value of 8.6 mm. For the second tunnel (RL), the computed settlement was 7.2 mm, compared with the measured settlement of 6.5 mm, indicating a strong correlation between the predicted and measured results. Furthermore, the model accurately captured the differential settlements, with computed values of 2.5 mm for tunnel LL and 4.7 mm for tunnel RL, closely matching the field measurements of 2.3 and 4.4 mm, respectively. Therefore, the numerical model was deemed reliable.

Additionally, a considerable increase in the maximum settlement was observed following the 180-day period of soil consolidation. The computed maximum settlement increased by 6.2 mm during this period, which closely resembled the observed field increase of 5.9 mm. This highlighted the significant role of soil consolidation in the additional settlement of piled buildings, which will be explored in further detail later.

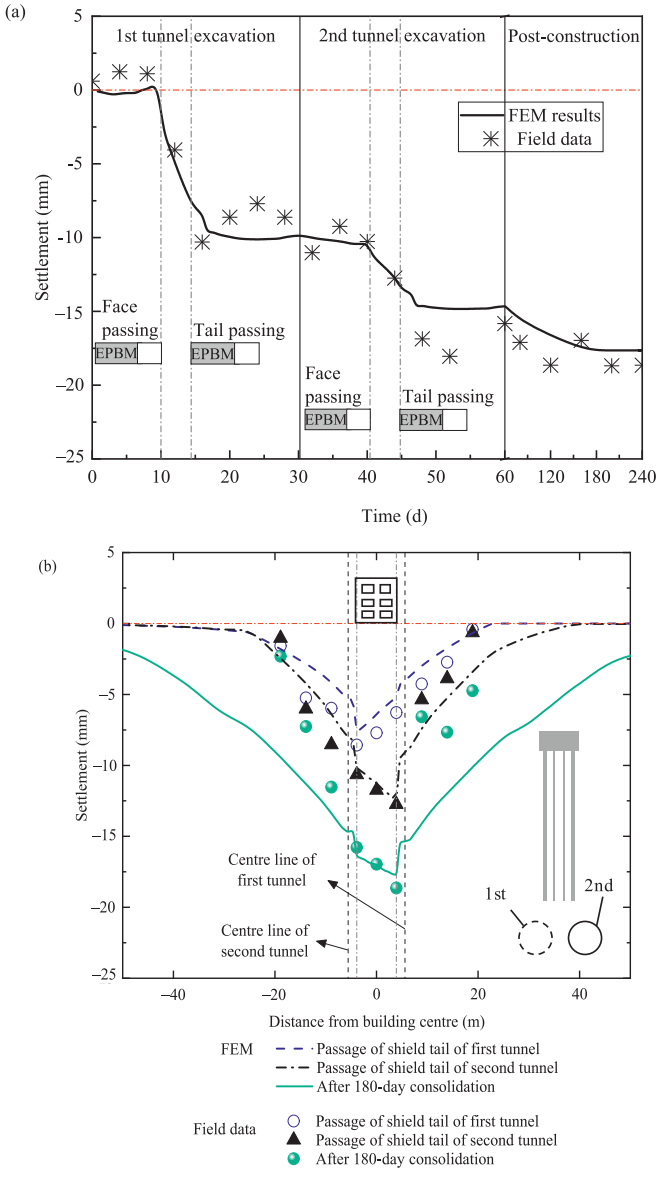

Fig. 6. Comparisons of the computed and measured settlements. (a) Time history curve of the maximum settlement of the piled building, and (b) settlement of the piled building.

3.3 Variations in pile toe resistance and pile shaft resistance

Figure 7 illustrates the variation rates of the pile toe resistance Q_b and pile shaft resistance Q_s for each pile at the monitoring section depicted in Fig. 2 during twin tunnelling. Four piles are named #1 to #4 from left to right.

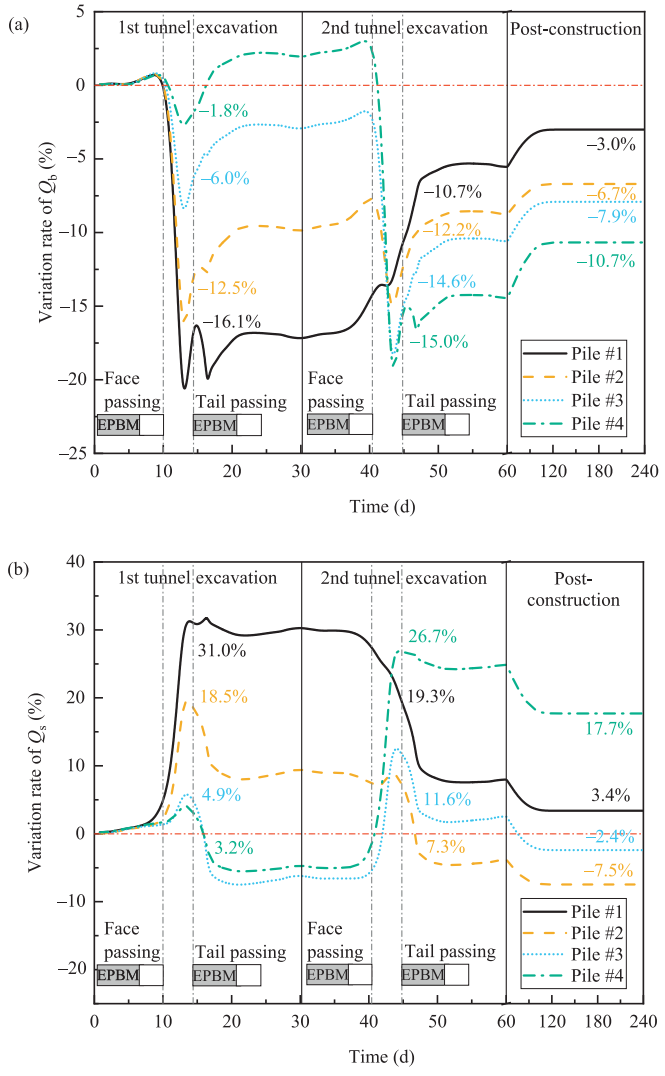

Fig. 7. Variation rates of (a) Q_b and (b) Q_s for each pile during twin tunnelling.

Pile #1 was positioned closest to the centreline of the first tunnel LL, and pile #4 was nearest to the centreline of the second tunnel RL. Q_b for all four piles decreased, and Q_s increased during the passage of the first tunnel. Notably, pile #1 experienced the most significant changes, with Q_b decreasing by a maximum of 16.1% and Q_s increasing by up to 31.0%.

It is important to note that the distance from the centre of the first tunnel to pile #1 was equal to the distance from the centre of the second tunnel to pile #4, as the twin tunnel was symmetrically located with respect to the piled building. As shown in Fig. 7(a), during the passage of the second tunnel, for pile #4, which was the closest to the second tunnel, Q_b decreased by 16.8% from the beginning of the second tunnel construction until the shield tail passed the monitoring section. This reduction was slightly greater than the 16.1% reduction observed for pile #1 during the passage of the first tunnel. Conversely, for pile #1, which was farthest from the second tunnel, Q_b exhibited a significant increase, with its value increasing from −17.2% to −10.7%. For the remaining piles (piles #2 and #3), the reductions in Q_b were smaller than those caused by the first tunnelling (piles #3 and #2). Meanwhile, as shown in Fig. 7(b), for pile #4, the increase in Q_s was slightly greater than that for pile #1 during the passage of the first tunnel. However, the increases in Q_s for the other piles (piles #2 and #3) were smaller than those caused by the first tunnelling (piles #3 and #2). Notably, the Q_s value for pile #1 decreased significantly.

As the shield tail passed, the monitoring section gradually entered the consolidation phase. During this phase, Q_b consistently increased, whereas Q_s consistently decreased. Hence, an increase in Q_b was accompanied by a decrease in Q_s, and vice versa. Additionally, the level of Q_b for pile #4, which was closest to the second tunnel, was the lowest among all the piles. As the distance from the second tunnel increased, the reduction in Q_b became less pronounced. This trend corresponded to the consolidation settlement pattern depicted in Fig. 6(b), where the building settlement on the side of the second tunnel exceeded that on the side of the first tunnel. This indicated a strong correlation between variations in the pile foundation load and the settlement of the piled building.

4 Parametric investigation of shield tunnelling parameters on soil behaviour

4.1 Simulating cases

To investigate the long-term response of piled buildings to shield tunnelling, various tunnelling parameters were varied in the numerical simulation. The cover depth C_d and centre-to-centre spacing of the two tunnels were set to $5D$ and $0.5D$, respectively, with both tunnels being excavated beneath the piled building.

According to Liu (2014) and Jeon et al. (2020), the face pressure P_f and grouting pressure P_g are critical tunnelling parameters that significantly influence the settlement behaviour of piled buildings during shield tunnel excavation. σ_{zz} denotes the vertical earth pressure at the tunnel centre, and σ_{xx} symbolizes the lateral earth pressure at the identical location. It is hypothesized that the benchmark face pressure P_{bf} corresponds to σ_{xx}, whereas the benchmark grouting pressure P_{bg} corresponds to σ_{zz}. The definitions of P_{bf} and P_{bg} are presented in Table 3. Variations in P_f were methodically selected as 80%, 90%, 110%, 120%, and 130% of P_{bf}. Similarly, variations in P_g were methodically selected as 80%, 90%, 110%, 120%, 130%, 150%, 160%, 180%, and 200% of P_{bg}. To thoroughly investigate the soil behaviour resulting from the sequential excavation of the first and second tunnels, the numerical simulations were categorized into two distinct groups.

Table 3
Definitions for the benchmark face pressure (P_{bf}) and grouting pressure (P_{bg}).

Parameter	Definition
Benchmark face pressure (P_{bf})	Set equal to the lateral earth pressure (σ_{xx}) at the tunnel centre
Benchmark grouting pressure (P_{bg})	Set equal to the vertical earth pressure (σ_{zz}) at the tunnel centre

Group 1: This group focused exclusively on simulating the construction of the first tunnel, with no involvement of a second tunnel. Upon completion of the first tunnel, a 10-year consolidation period was initiated to evaluate the soil settlement and structural response over an extended duration.

Group 2: In this setup, both tunnels were excavated sequentially, with no delay between the construction of the first and second tunnels. This arrangement enabled

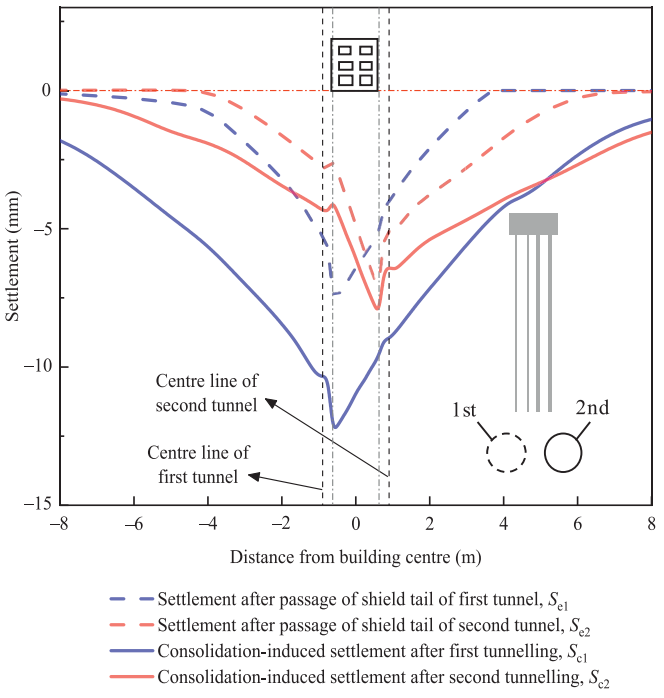

Fig. 8. Comparison of piled building settlements induced by tunnelling and consolidation of the first and second tunnels.

the assessment of additional displacement of the piled buildings caused by the second tunnel. The additional displacement was determined by subtracting the displacement resulting from the first tunnelling from that observed after the excavation of both tunnels. Furthermore, a 10-year consolidation period was also applied to analyse the long-term responses of piled buildings, specifically focusing on the effects of soil consolidation.

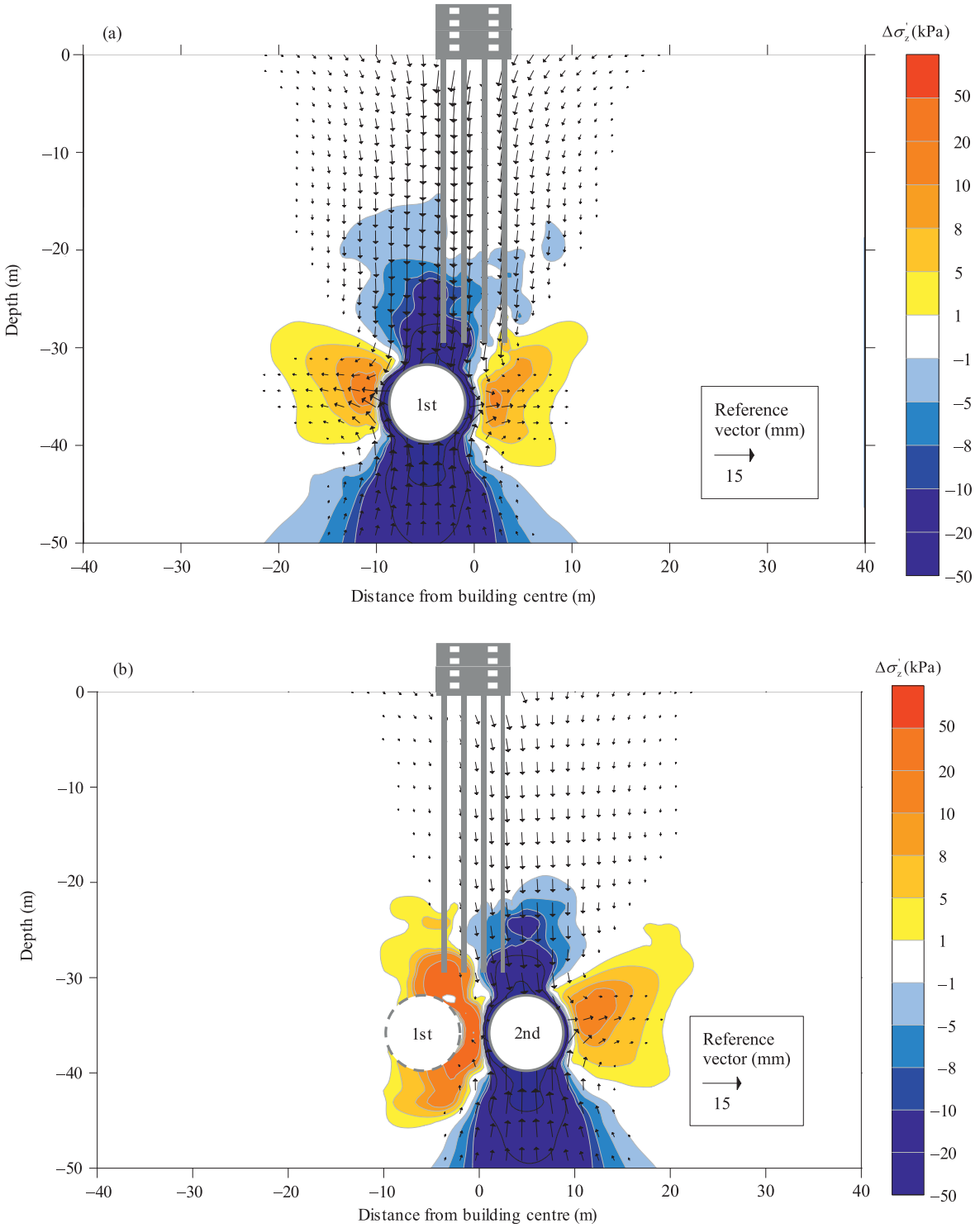

Fig. 9. Variations in vertical soil stress induced by tunnelling. (a) First tunnel, and (b) second tunnel.

4.2 Comparisons of short-term and long-term response of piled building induced by shield tunnelling

Figure 8 provides a comparative analysis of the surface settlements resulting from tunnelling and subsequent consolidation for the first and second tunnels. The surface settlements recorded immediately after the passage of the shield tail in the first and second tunnels are denoted as S_{e1} and S_{e2}, respectively. Similarly, the surface settlements observed after a 10-year consolidation period post-tunnelling for the first and second tunnels are denoted as S_{c1} and S_{c2}, respectively.

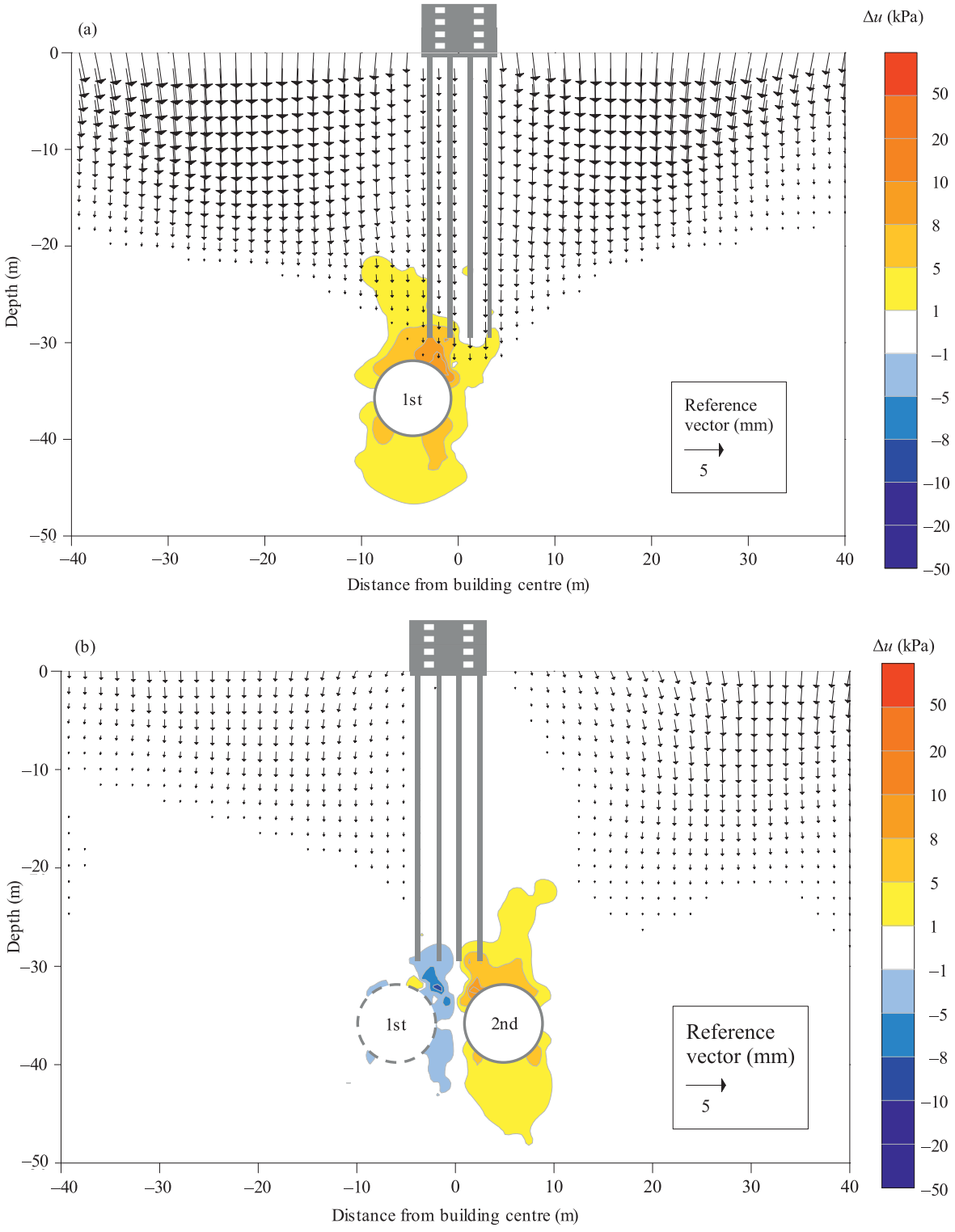

Fig. 10. Variations in pore pressure induced by soil consolidation. (a) First tunnel, and (b) second tunnel.

During the passage of the twin tunnel, the maximum S_{e2} of 7.2 mm induced by the second tunnel was slightly lower than the maximum S_{e1} (7.6 mm) caused by the first tunnel. The differential settlement caused by the second tunnel (4.7 mm) exceeded that caused by the first tunnel (2.5 mm). During the consolidation phase, the maximum S_{c2} (8.1 mm) was considerably smaller than the maximum S_{c1} (12.3 mm), indicating distinct long-term consolidation behaviours between the two tunnels. Additionally, the differential settlements of S_{c1} and S_{c2} were essentially the same as those of S_{e1} and S_{e2}.

Figure 9 illustrates the variations in the vertical soil stress induced by tunnelling. During the construction of the first tunnel, the soil between the tunnel crown and pile toe underwent an unloading effect owing to the excavation, resulting in the most significant reduction in the vertical stress beneath pile #1, which was closest to the first tunnel. As the distance between the pile and the center of the first tunnel increased, the reduction in the vertical stress at the pile toe diminished gradually (Fig. 9(a)).

During the construction of the second tunnel, the vertical stress increment in the soil between the two tunnels was more pronounced than that in the first tunnel. As shown in Fig. 7 (a), during the construction of the first tunnel, the pile toe resistances (Q_b) of all piles exhibited a decreasing trend. However, during the construction of the second tunnel, the piles closer to that (piles #3 and #4) also experienced a reduction in Q_b with a magnitude comparable to that

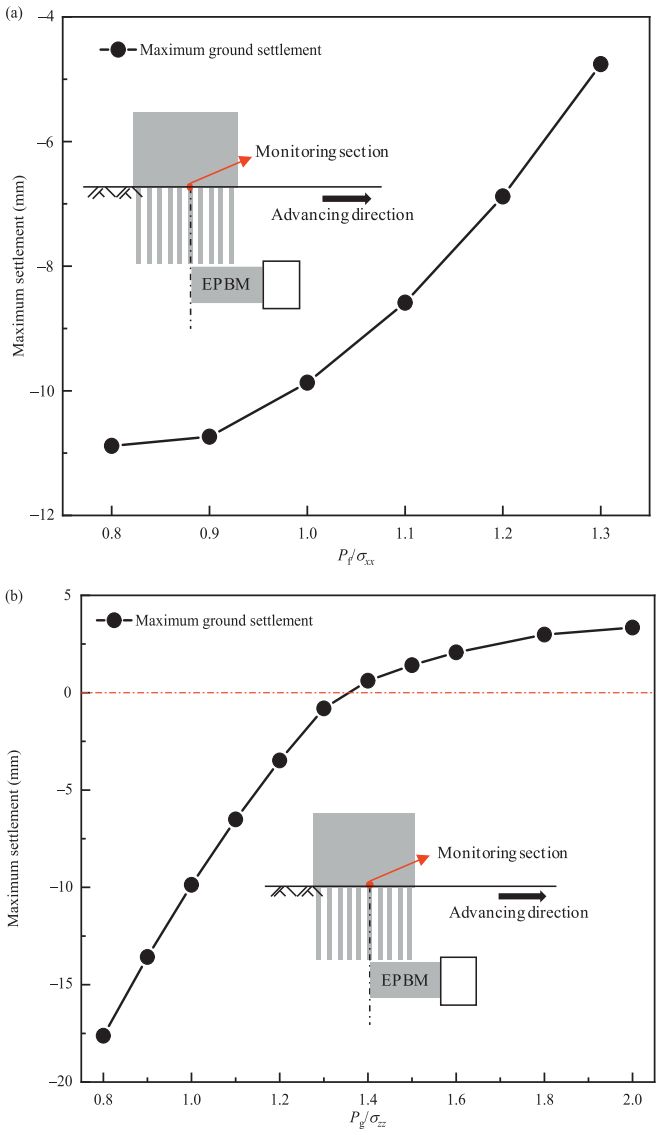

Fig. 11. Maximum settlement of piled buildings after tail passage in relation to various tunnelling parameters. (a) Face pressure, and (b) grouting pressure.

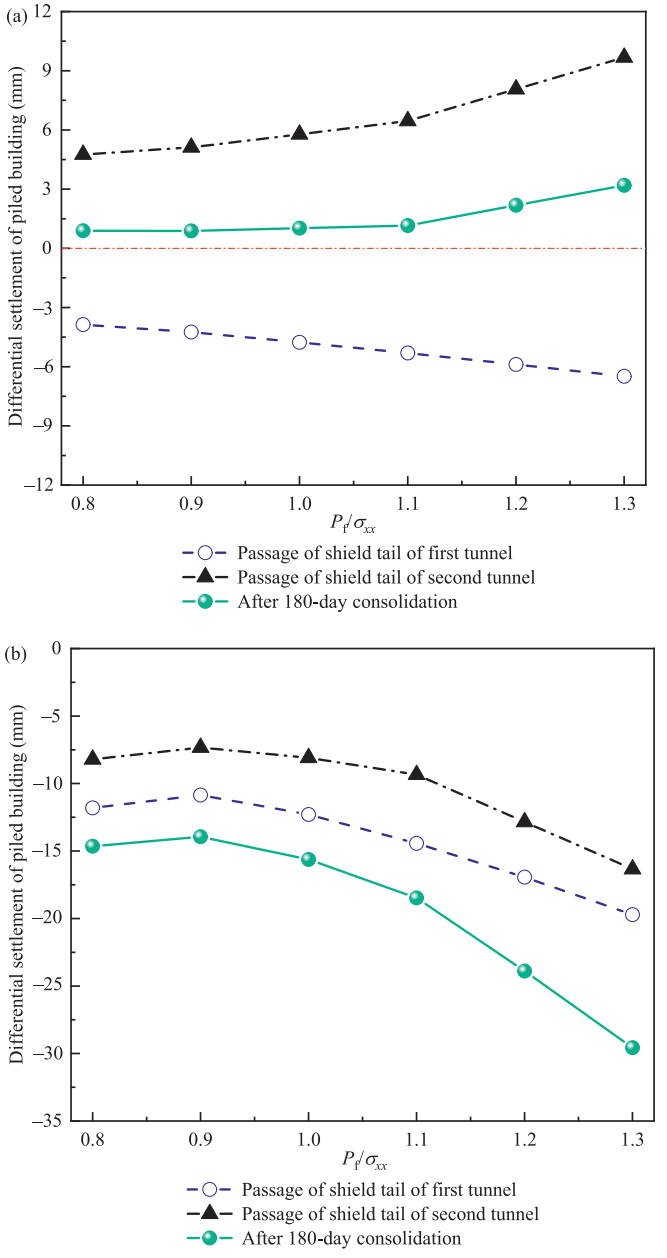

Fig. 12. (a) Differential settlements, and (b) maximum displacement of piled buildings in relation to P_f.

induced by the first tunnel. By contrast, the piles closer to the first tunnel (piles #1 and #2) exhibited an increase in Q_b.

This suggests that the construction of the second tunnel not only induced a more significant increase in the vertical stress within the soil between the two tunnels due to the sheltering effect of the first tunnel, amplifying the loading effect, but also enhanced the bearing capacity of the pile foundations in this region. Additionally, the excavation of the first tunnel induced stress relief in the soil above its crown, forming a zone of reduced vertical and lateral stresses. When the second tunnel was excavated, it interacted with this disturbed soil, which had already experienced stress relief. Consequently, the additional stress perturbations in the soil above the crown of the first tunnel caused by the second tunnel were less significant, resulting in a reduced settlement compared with those induced by the first tunnel. Consequently, the settlement of the piled building and ground settlement of the adjacent structures were predominantly localized in the unloading zone directly above the crown of the second tunnel, as shown in Fig. 9(b).

To examine the variations in consolidation settlement induced by the construction of the first and second tunnels, Fig. 10 illustrates the distributions of excess pore pressure (Δu) and soil consolidation settlement after the passage of the shield tail for both tunnels. Figure 10(a) depicts the consolidation settlement and excess pore pressure distribution in the soil after the passage of the shield tail of the first tunnel. Figure 10(b) shows the consolidation settlement attributable solely to the second tunnel, which was calculated by subtracting the settlement induced by the first tunnel from the total settlement of the twin tunnels. Similarly, the excess pore pressure distribution caused exclusively by the second tunnel was obtained by subtracting the excess pore pressure generated by the first tunnel from that of the twin tunnel.

As shown in Fig. 10, positive values of relative excess pore pressure indicate that the excess pore pressure in the soil after the passage of the shield tail of the second tunnel exceeded that induced by the first tunnel, termed "positive relative excess pore pressure". Conversely, negative values signify that the excess pore pressure was lower than that caused by the first tunnel, termed "negative relative excess pore pressure".

The surrounding soil underwent consolidation after the shield tail passed through the first tunnel. The positive excess pore pressure dissipated progressively near the tunnel crown. This dissipation increased the effective stress of the soil. As the effective stress increased, the soil was compressed, inducing consolidation settlement in the piled buildings above the tunnel, as shown in Fig. 8.

As illustrated in Fig. 10(b), the passage of the shield tail of the second tunnel induced a negative relative excess pore water pressure in the spring line region of the first tunnel proximate to the side of the second tunnel. This phenomenon was observed in the soil zone beneath the pile toe of the pile foundation. The development of negative relative excess pore water pressure signified that the excavation of the second tunnel modified the stress state of the soil surrounding the first tunnel, leading to a reduction in the excess pore pressure in this region. Consequently, when the consolidation settlement induced solely by the second tunnel was evaluated, the dissipation of the excess pore pressure in the region exhibiting negative relative excess pore pressure diminished compared with the scenario of a single-tunnel excavation. This reduction effectively mitigated the consolidation settlement of the piled buildings following the completion of the second tunnel. As shown in Fig. 8, the consolidation settlement resulting from the second tunnel was markedly less pronounced than that induced by the first tunnel.

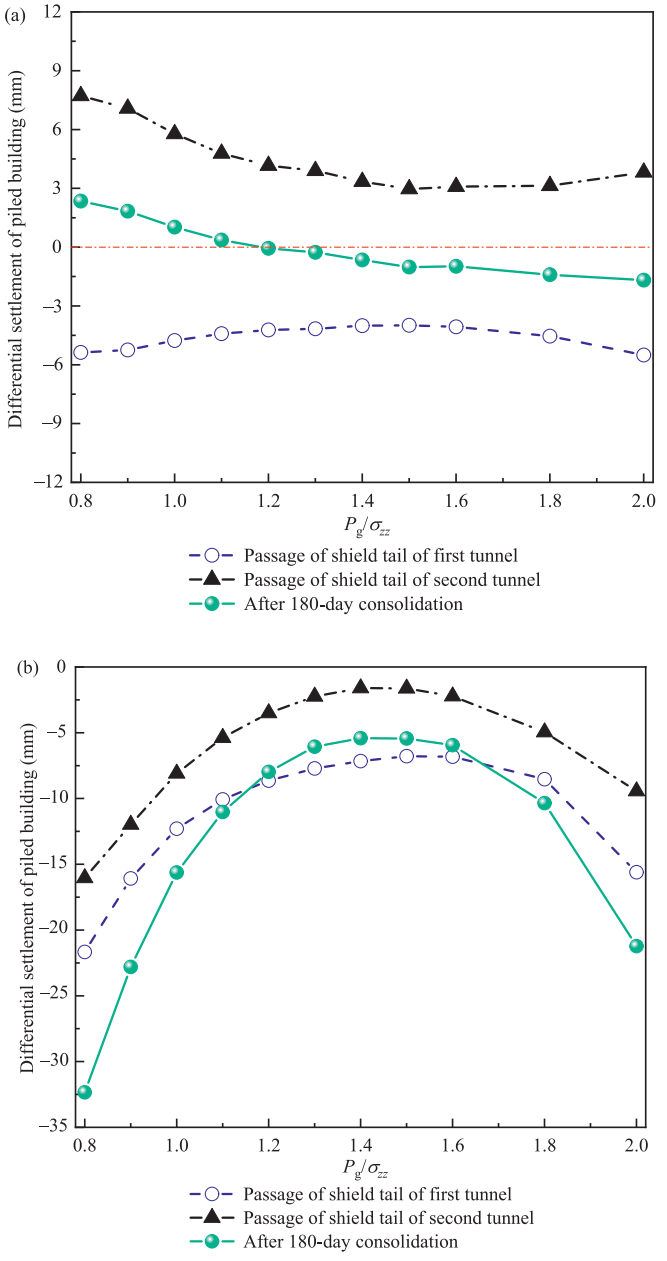

Fig. 13. (a) Differential settlements, and (b) maximum displacements of piled building in relation to P_g.

4.3 Long-term ground settlement induced by shield tunnelling

Figure 11 illustrates the relationship between the maximum settlement of the piled building immediately after the passage of the shield tail (short-term settlement) and the varying tunnelling parameters. The data revealed a progressive decrease in maximum settlement with increasing face and grouting pressures. Furthermore, given the observed differences in consolidation settlements between the first and second tunnels, as detailed in Fig. 8, the relationship between the consolidation-induced long-term settlement and these tunnelling parameters requires further detailed investigation to comprehensively understand their interdependencies.

Figure 12 shows the maximum long-term displacement and differential settlement of the piled building influenced by varying levels of P_f. The twin tunnel was positioned directly beneath the piled building and symmetrically aligned with the centreline of the building to ensure a consistent experimental setup. In this study, a clockwise inclination of the piled building was considered positive.

As shown in Fig. 12, for both the first and second tunnels, the maximum displacement reached its lowest value when P_f was set to 90% of the benchmark face pressure, P_{bf}, and it progressively increased as P_f deviated from this value. Additionally, the differential settlement of the piled building increased as P_f increased. During the construction of the first tunnel, the piled building was inclined towards the first tunnel. The differential settlement induced by the second tunnel was significantly greater than that induced by the first tunnel. The cumulative differential settlement remained positive in all the cases and continued to increase with increasing P_f. When P_f ranged from 80% to 100% of P_{bf}, the inclination of the piled building became negligible, as shown in Fig. 12.

Figure 13 illustrates the influence of varying P_g values on the maximum long-term displacement and differential settlement of the piled building. The observed trend shows that

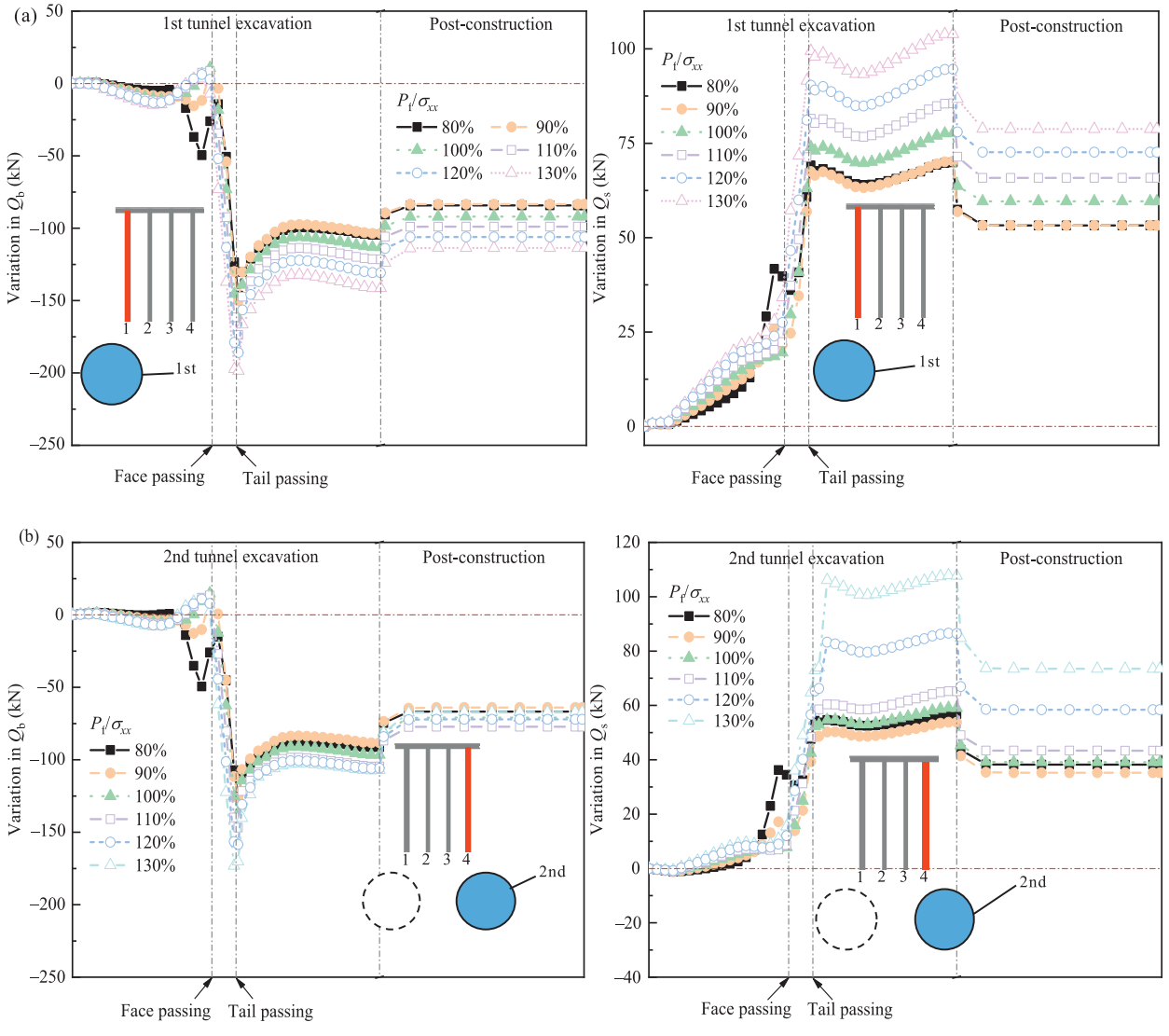

Fig. 14. Variations in Q_b and Q_s for piles closest to the tunnel under excavation in relation to P_f. (a) First tunnel, and (b) second tunnel.

the maximum displacement initially decreased before increasing with ascending P_g levels, reaching its lowest point when P_g was set to 150% of the benchmark grouting pressure P_{bg}. This P_g level also corresponded to the minimal differential settlement observed in the piled building. Conversely, when P_g was less than or twice the vertical earth pressure, both the settlement and inclination of the piled building increased significantly. Specifically, at a P_g of 80% of P_{bg}, the maximum displacement peaks at approximately 21.7 mm, which was the highest observed across all scenarios. Moreover, when P_g ranged from 120% to 160% of P_{bg}, the piled building experienced heaving induced by the second tunnelling, leading to a reduction in the accumulated settlement. The building inclination shifted from negative to positive at a P_g of 120% of P_{bg}, with the inclination value remaining less than 1 mm within 120%–160% of P_{bg}. This preliminary assessment provides foundational guidelines for optimizing tunnelling parameters, though further research and validation may be necessary to refine these recommendations.

4.4 Variations in soil stress induced by shield tunnelling

4.4.1 Influence of face pressure

Figure 14 illustrates the variations in pile toe resistance Q_b and pile shaft resistance Q_s for piles located closest to the tunnel under excavation in relation to P_f. As the tunnel face approached, a slight increase in Q_b was observed, followed by a decrease toward the passage of the shield tail, indicating a reduction in the pile toe stability. Concurrently, Q_s experienced a consistent increase, reflecting the enhanced pile shaft friction. After the shield tunnel passed beneath the piled building, a recovery phase for Q_b ensued, which gradually stabilized over a 10-year consolidation period. In parallel, Q_s began to decrease, eventually levelling off during the same consolidation phase, suggesting the stabilization of soil-pile interactions. Notably, Q_b and Q_s displayed a clear inverse correlation throughout the tunnelling process. An increase in Q_b typically corresponded to a decrease in Q_s and vice versa. This pattern likely reflected a load-transfer mechanism within the piles, where

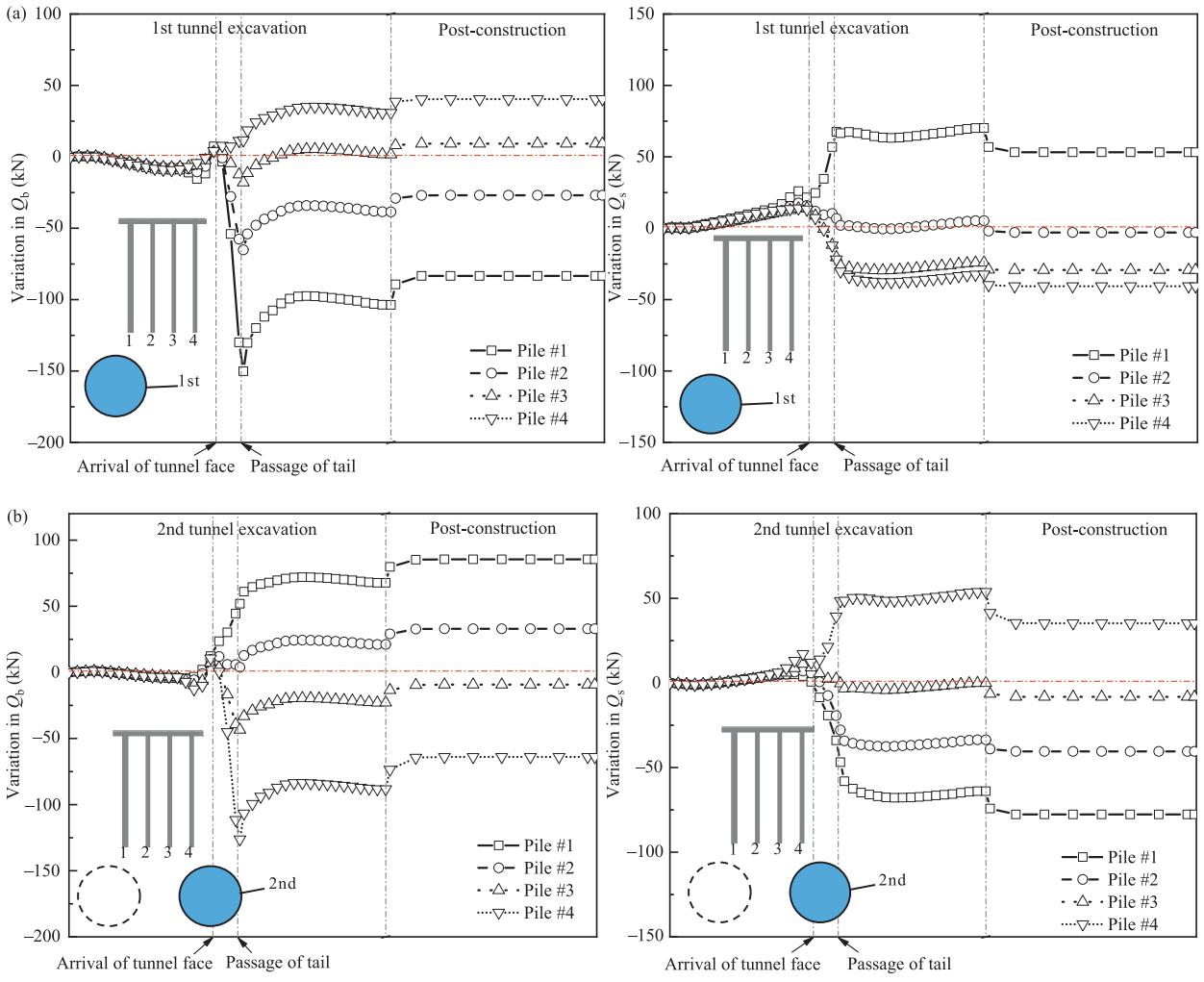

Fig. 15. Variations in Q_b and Q_s for each pile (P_f is set to 90% of P_{bf}). (a) First tunnel, and (b) second tunnel.

shifts in the structural load were redistributed between the toe and shaft of the piles. For both the first (Fig. 14(a)) and second tunnels (Fig. 14(b)), setting P_f to 90% of P_{bf} resulted in minimal decreases in Q_b and maximal increases in Q_s following soil consolidation, which was consistent across all observed cases. This minimal reduction in Q_b correlated directly with the reduced settlement observed in piled buildings, suggesting that maintaining P_f at this level optimally mitigated settlement effects.

Figure 15 shows the variations in Q_b and Q_s for each pile (piles #1–#4) when P_f was set to 90% of P_{bf}. For the first tunnel, as illustrated in Fig. 15(a), Q_b decreased for piles #1 and #2, whereas it increased for piles #3 and #4. Q_s increased for pile #1, while Q_s decreased for piles #3 and #4. The variation in Q_s for pile #2 was negligible.

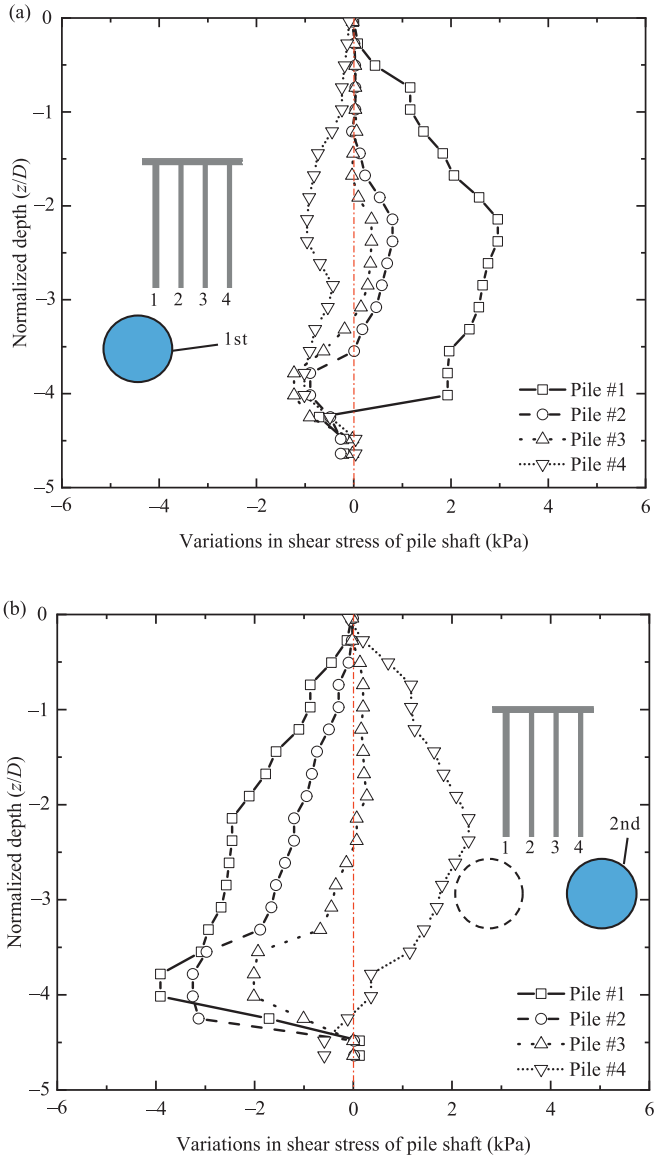

Fig. 16. Shear stress variations along the shaft of each pile during the consolidation phase (P_f is set to 90% of P_{bf}). (a) First tunnel, and (b) second tunnel.

For the second tunnel, as shown in Fig. 15(b), pile #4 exhibited a response similar to pile #1 during the first tunnelling, indicating the consistent impact of tunnelling at similar proximities. In this case, Q_b decreased for piles #3 and #4, albeit with a less pronounced decrease than for the first tunnelling. Conversely, Q_b for piles #1 and #2 exhibited a greater increase than that observed previously. Q_s for the second tunnelling exhibited a smaller increase for pile #4 and a more significant decrease for piles #1 and #2 compared with the first tunnelling. This pattern suggests that the lesser reduction in Q_b for piles located closer to the second tunnel may contribute to the observed outcome, where the long-term settlement of the piled building induced by the second tunnelling was less than that caused by the first tunnelling.

Figure 16 shows the variations in shear stress within the pile shafts for each pile (piles #1–#4), under conditions where P_f was set to 90% of P_{bf}. The load-transfer mechanism of the pile foundation, as shown in Fig. 17, was derived by combining the changes in Q_b from Fig. 15 and the redistribution of the shear stress within the pile shafts, as shown in Fig. 16. The detailed depiction reveals that the shear stress was significantly higher for the pile located closest to pile #1 during the first tunnelling and pile #4 during the second. However, the increase in the shear stress was not uniform along the length of the pile. During the consolidation phase of the first tunnel, the lower portions of piles #1 and #2 experienced a decrease in shear stress coupled with a decreased Q_b for these piles (Fig. 15(a)).

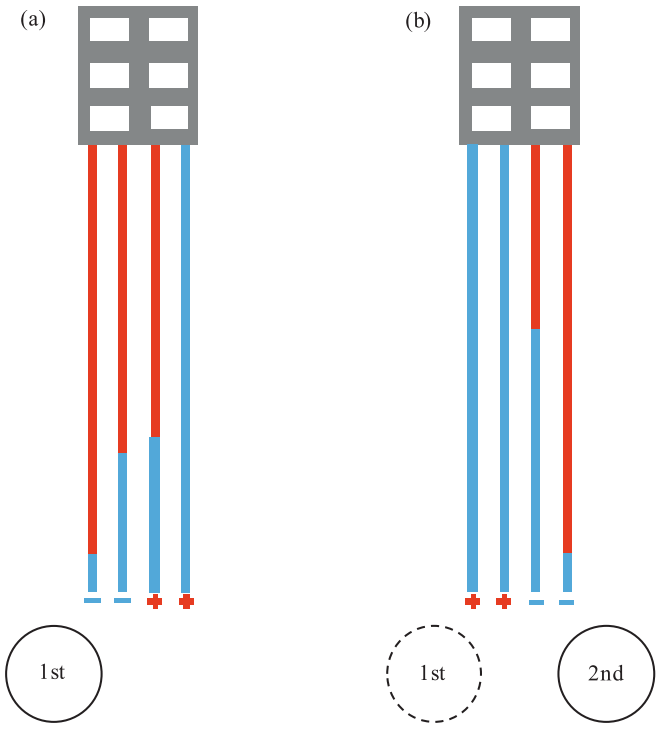

Fig. 17. Schematic of the load transfer mechanism for first and second tunnels during the consolidation phase (P_f is set to 90% of P_{bf}). (a) First tunnel, and (b) second tunnel.

The decreased shear stress in the lower shaft portion was correlated with the increased shear stress in the upper shaft portion. Additionally, the extent of this decrease in the shear stress in the pile shaft increased as the distance from the tunnel increased. For piles #3 and #4 for the first tunnelling, the decreased load within the pile shaft was transferred to the pile toe resistance, indicating a redistribution of structural loads. Similarly, Zheng et al. (2023) reported that the load initially carried by the pile toe was transferred to the pile shaft, which was consistent with the load redistribution observed in this study.

During the consolidation phase of the second tunnel, piles #3 and #4, positioned within the unloading region caused by the second tunnel, experienced a decreased load in both the pile toe and the lower shaft portion, with an increased load observed in the upper portion of the shaft. Conversely, for the remaining piles (piles #1 and #2) in the case of the second tunnelling, Q_b generally increased (Fig. 15(b)), accompanied by a corresponding decrease in shear stress across the entire pile shaft.

4.4.2 Influence of grouting pressure

Figure 18 shows the variations in Q_b and Q_s for the piles located closest to the tunnel under excavation in relation to P_g. The variation in Q_b was notably influenced by the passage of the shield tail, exhibiting a gradual increase as P_g increased. After the completion of shield tunnelling, during a 10-year consolidation period, the previously observed reduction in Q_b began to recover. Conversely, the variations in Q_s displayed an inverse pattern to Q_b. As Q_b increased, Q_s decreased. This inverse relationship likely reflected a load-transfer mechanism within the pile structure, where shifts in the structural load were redistributed between the toe and shaft of the pile. For both the first (Fig. 18(a)) and second tunnels (Fig. 18(b)), setting P_g to 150% of P_{bg} resulted in minimal decreases in Q_b and

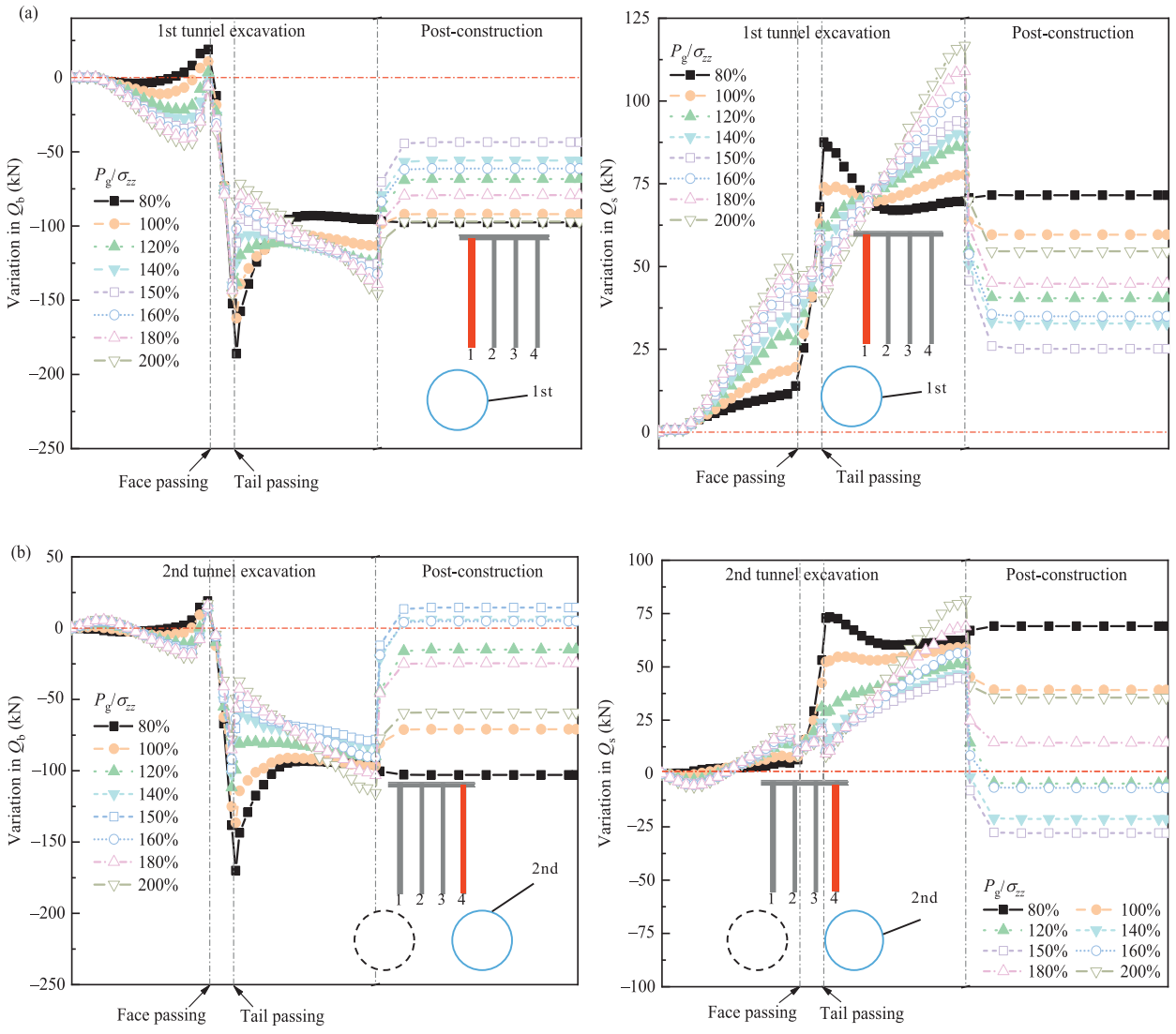

Fig. 18. Variations in Q_b and Q_s for piles closest to the tunnel under excavation in relation to P_g. (a) First tunnel, and (b) second tunnel.

maximal increases in Q_s after soil consolidation, which was consistent across all observed cases. This modest reduction in Q_b was directly correlated with the reduced settlement observed in the piled building.

Figure 19 shows the variations in Q_b and Q_s for each pile (piles #1–#4) when P_g was set to 150% of P_{bg}. For the first tunnel, as shown in Fig. 19(a), the decrease in Q_b for piles #1 and #2 was notably more subdued than the previous observations from Fig. 15(a), whereas the increase in Q_b for piles #3 and #4 was significantly more pronounced. For the second tunnel, as shown in Fig. 19(b), a consistent pattern was observed for all piles, characterized by an increase in Q_b and a concurrent decrease in Q_s. This uniform response across all piles suggested a stabilization of the pile foundation when P_g was set to 150% of P_{bg}. Furthermore, this increase in Q_b contributed to the heaving of the piled building.

Figure 20 shows the variations in shear stress within the pile shafts for each pile (piles #1 to #4), when P_g was set to 150% of P_{bg}. The load-transfer mechanism of the pile foundation, as shown in Fig. 21, was derived by combining the changes in Q_b from Fig. 19 and the redistribution of the shear stress within the pile shafts, as shown in Fig. 20. During the consolidation phase of the first tunnel, consistent with the observations in Fig. 16(a), the shear stress at the lower portions of the pile shafts decreased uniformly across all the piles. The range of the reduced shear stress gradually expanded as the distance between the pile and tunnel increased. For piles #1 and #2, which were adjacent to the first tunnel, both Q_b and the shear stress at the lower portions of the pile shafts decreased, leading to the transfer of load to the upper portions of the pile shafts. Notably, as shown in Fig. 19(a), for pile #1, which was the closest to the first tunnel, Q_s increased. This indicated that load transfer predominantly occurred in pile #1, with the load shifting from the pile toe to the pile shaft. For piles #3 and #4, located farther from the first tunnel, Q_b increased, whereas the shear stress of the entire pile shaft decreased. The load was then transferred from the pile shaft to the pile toe.

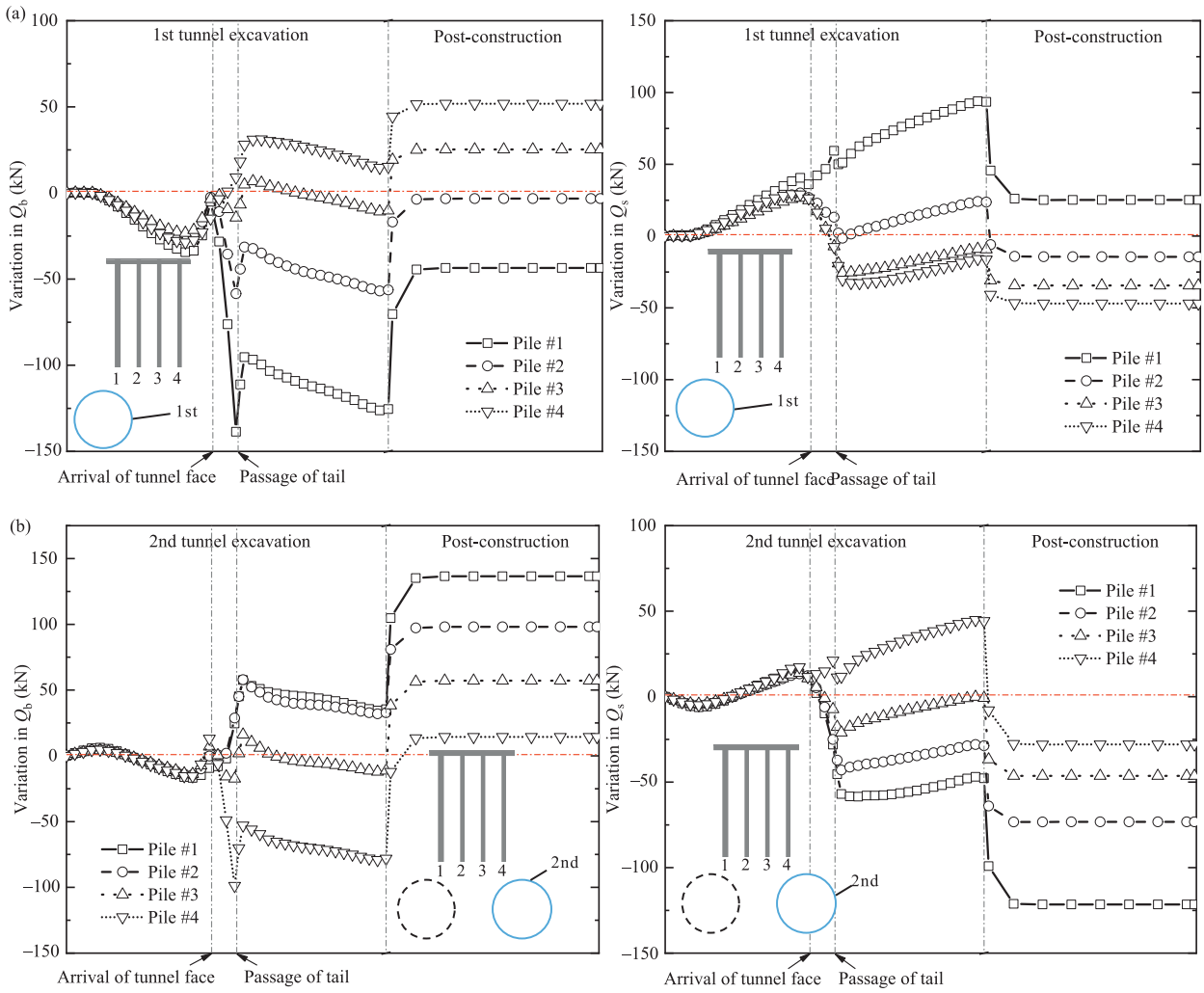

Fig. 19. Variations in Q_b and Q_s for each pile (P_g is set to 150% of P_{bg}). (a) First tunnel, and (b) second tunnel.

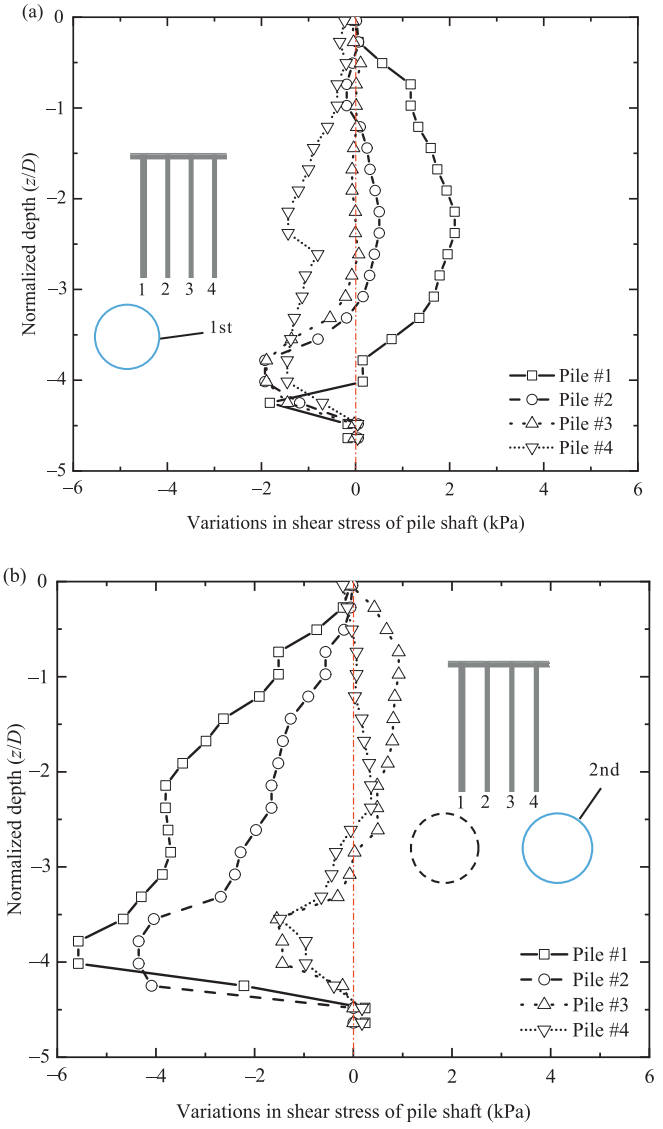

Fig. 20. Shear stress variations along the shaft of each pile during the consolidation phase (P_g was set to 150% of P_{bg}). (a) First tunnel, and (b) second tunnel.

During the consolidation phase of the second tunnel, as shown in Figs. 19(b) and 20(b), all piles exhibited a decrease in shear stress across the pile shafts. For any given pile, the load was transferred from the pile shaft to the pile toe. Notably, for pile #1, which was the farthest from the second tunnel, Q_b exhibited the most significant increase, whereas the shear stress along the entire pile shaft showed the greatest decrease. This suggests that the load transfer primarily occurred in pile #1, with the load shifting from the pile shaft to the pile toe. Zheng et al. (2023) reported a different load-transfer mechanism, stating that the load initially carried by the pile toe is transferred to the pile shaft during tunnelling activities. This discrepancy highlights the distinct influence of the consolidation phase and the applied grouting pressure level, which effectively enhances Q_b and mitigates long-term settlement.

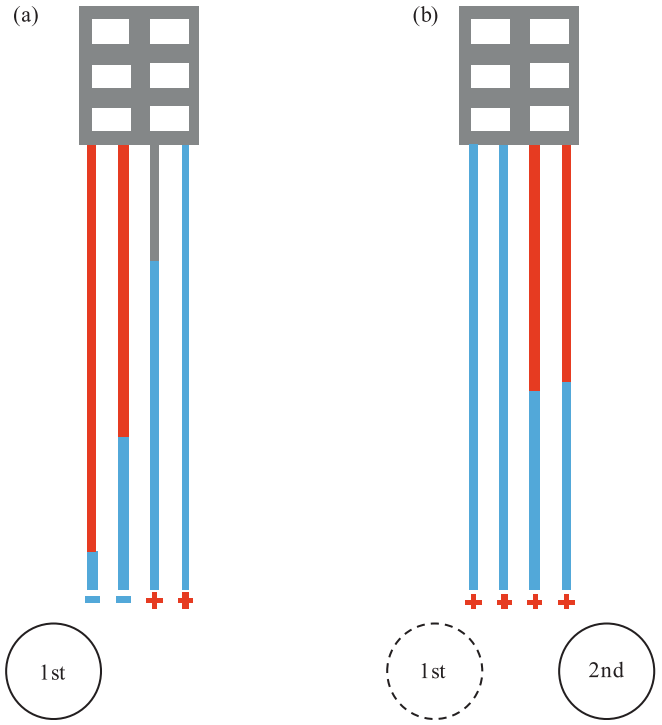

Fig. 21. Schematic of load transfer mechanism for first and second tunnels during the consolidation phase (P_g was set to 150% of P_{bg}). (a) First tunnel, and (b) second tunnel.

5 Conclusions

This study examined the long-term soil behaviour resulting from sequential shield tunnelling by employing an advanced three-dimensional numerical model to probe the complex interactions between the tunnel, surrounding soil, and adjacent pile foundations. Specifically, tailored to evaluate the effects of soil consolidation after tunnel construction, this study addressed a crucial aspect affecting the stability and durability of underground infrastructure. The objective was to meticulously assess the influence of critical tunnelling parameters and to delineate the optimal settings for their practical application. Furthermore, the investigation provided a detailed analysis of the load transfer mechanisms within piled buildings, which are significantly influenced by these essential tunnelling parameters. The study arrived at several conclusive insights based on the scrutiny of tunnelling conditions.

(1) The variations in Q_b and Q_s crucially influence the structural behaviour of a piled building, with the greatest displacement occurring where Q_b is most significantly reduced. For instance, during the first tunnelling, the toe resistance of the pile closest to the centre line of the first tunnel decreases most significantly, resulting in an inclination toward the first tunnel.
(2) For both the first and second tunnels, when P_f is set to 90% of P_{bf}, the reduction in Q_b for the piles closest to the excavated tunnel is minimal, and the maximum

consolidation settlement of the piled buildings reaches its lowest magnitude at this P_f level. For piles near the excavated tunnel (piles #1 and #2 during excavation of the first tunnel; piles #3 and #4 during excavation of the second tunnel), both Q_b and the shear stress at the lower portions of the pile shafts decrease, whereas the shear stress at the upper portions increases, indicating a load transfer from the pile toe to the pile shaft. In contrast, for piles farther from the excavated tunnel (piles #3 and #4 during the excavation of the first tunnel; piles #1 and #2 during the excavation of the second tunnel), Q_b increases, whereas the shear stress along the entire pile shaft decreases, suggesting a load transfer from the pile shaft to the pile toe. The variations in Q_b and Q_s are inversely related. An increase in Q_b corresponds to a decrease in Q_s and vice versa.

(3) When P_g is set between 120% and 160% of P_{bg}, the maximum consolidation settlement of the piled buildings caused by twin tunnelling is smaller than that induced by the individual construction of the first tunnel. This indicates that within this grouting pressure range, the construction of the second tunnel results in building heave and an inclination towards the direction of the first tunnel, with the differential settlement remaining below 1 mm. For both the first and second tunnels, when P_g is 150% of P_{bg}, the reduction in Q_b of the pile closest to the excavated tunnel is the smallest. Notably, for the second tunnel, the grouting pressure causes Q_b to shift from decreasing to increasing, resulting in building heave. At this P_g level, Q_b increases for all piles. For the piles adjacent to the second tunnel (piles #3 and #4), the shear stress at the lower portions of the pile shafts decreases, whereas both Q_b and the shear stress at the upper portions increase. Consequently, the load is transferred from the lower portions of the pile shafts to both the pile toe and the upper portions of the pile shafts. For the piles farther from the second tunnel (piles #1 and #2), Q_b increases, whereas the shear stress along the entire pile shaft decreases, as the load is transferred from the pile shaft to the pile toe.

Data availability

The data that support the findings of this study are available from the corresponding author upon reasonable request.

CRediT authorship contribution statement

Ruikun Wang: Writing – review & editing, Writing – original draft, Software, Investigation, Formal analysis. **Gang Zheng:** Supervision, Methodology, Conceptualization. **Huayang Lei:** Supervision, Methodology, Formal analysis. **Xuesong Cheng:** Supervision, Methodology, Investigation, Funding acquisition. **Eng-Choon Leong:** Validation, Supervision, Software. **Yetao Ji:** Data curation.

Declaration of competing interest

The authors declare that they have no known competing financial interests or personal relationships that could have appeared to influence the work reported in this paper.

Acknowledgement

The authors would like to acknowledge the financial support from the National Natural Science Foundation of China (Grant No. 52178343), Science Fund for Distinguished Young Scholars of Tianjin Municipality (Grant No. 24JCJQJC00170), and the Innovative Research Group Project of the National Natural Science Foundation of China (Grant No. 52421005).

References

Boonyarak, T., Phisitkul, K., Ng, C. W. W., Teparaksa, W., & Aye, Z. Z. (2014). Observed ground and pile group responses due to tunneling in Bangkok stiff clay. *Canadian Geotechnical Journal, 51*(5), 479–495.

Cao, L., Chen, X., Lin, X. T., Su, D., Fang, H., & Lu, D. (2023). Analytical solutions for the restraint effect of isolation piles against tunneling-induced vertical ground displacements. *Journal of Rock Mechanics and Geotechnical Engineering, 15*(10), 2582–2596.

Chen, R., Yin, X., Tang, L., & Chen, Y. (2018). Centrifugal model tests on face failure of earth pressure balance shield induced by steady state seepage in saturated sandy silt ground. *Tunnelling and Underground Space Technology, 81*, 315–325.

Cheng, C., Dasari, G., Chow, Y., & Leung, C. (2007). Finite element analysis of tunnel–soil–pile interaction using displacement controlled model. *Tunnelling and Underground Space Technology, 22*(4), 450–466.

Chore, H., Ingle, R., & Sawant, V. (2010). Building frame-pile foundation-soil interaction analysis: A parametric study. *Interaction and Multiscale Mechanics, 3*(1), 55–79.

Franza, A., & Marshall, A. M. (2018). Centrifuge modeling study of the response of piled structures to tunneling. *Journal of Geotechnical and Geoenvironmental Engineering, 144*(2), 04017109.

Franzius, J., & Potts, D. (2005). Influence of mesh geometry on three-dimensional finite-element analysis of tunnel excavation. *International Journal of Geomechanics, 5*(3), 256–266.

Gokuldas, S., Banerjee, S., & Nimbalkar, S. S. (2020). Effects of tunneling-induced ground movements on stability of piled raft foundation: Three-dimensional finite-element approach. *International Journal of Geomechanics, 20*(8), 04020104.

Hong, Y., Soomro, M. A., & Ng, C. W. W. (2015a). Settlement and load transfer mechanism of pile group due to side-by-side twin tunnelling. *Computers and Geotechnics, 64*, 105–119.

Hong, Y., Soomro, M. A., Ng, C. W. W., Wang, L., Yan, J., & Li, B. (2015b). Tunnelling under pile groups and rafts: Numerical parametric study on tension effects. *Computers and Geotechnics, 68*, 54–65.

Huang, F., Wang, Z., Zhang, M., & Li, S. (2022). Failure mechanism of the bearing stratum at the end of a pile induced by shield tunnel excavation beneath a piled building. *KSCE Journal of Civil Engineering, 26*(2), 942–954.

Jeon, Y. J., Jeon, S. C., Jeon, S. J., & Lee, C. J. (2020). Study on the behaviour of pre-existing single piles to adjacent shield tunnelling by considering the changes in the tunnel face pressures and the locations of the pile tips. *Geomechanics and Engineering, 21*(2), 187–200.

Jin, H., Yuan, D., Zhou, S., & Zhao, D. (2022). Short-term and long-term displacement of surface and shield tunnel in soft soil: Field observations and numerical modeling. *Applied Sciences, 12*(7), 3564.

Jongpradist, P., Kaewsri, T., Sawatparnich, A., Suwansawat, S., Youwai, S., Kongkitkul, W., & Sunitsakul, J. (2013). Development of tunneling

influence zones for adjacent pile foundations by numerical analyses. *Tunnelling and Underground Space Technology, 34*, 96–109.
Józefiak, K., Zbiciak, A., Maślakowski, M., & Piotrowski, T. (2015). Numerical modelling and bearing capacity analysis of pile foundation. *Procedia Engineering, 111*, 356–363.
Komiya, K., Takiyama, K., & Akagi, H. (2006). Settlement behaviour of a shield tunnel constructed in subsiding reclaimed area. In *Proceedings of the 5th International Conference on Geotechnical Aspects of Underground Construction in Soft Ground, the Netherlands* (pp. 239–244).
Lee, C. (2012). Numerical analysis of the interface shear transfer mechanism of a single pile to tunnelling in weathered residual soil. *Computers and Geotechnics, 42*, 193–203.
Liu, Y. L. (2014). Numerical analysis of the deformation law of deep foundation pit of subway station by FLAC3D. *Advanced Materials Research, 915*, 62–67.
Lu, H., Shi, J., Ng, C. W. W., & Lv, Y. (2020). Three-dimensional centrifuge modeling of the influence of side-by-side twin tunneling on a piled raft. *Tunnelling and Underground Space Technology, 103*, 103486.
Marshall, A. M. (2012). Tunnel-pile interaction analysis using cavity expansion methods. *Journal of Geotechnical and Geoenvironmental Engineering, 138*(10), 1237–1246.
Meng, F. Y., Chen, R. P., & Kang, X. (2018). Effects of tunneling-induced soil disturbance on the post-construction settlement in structured soft soils. *Tunnelling and Underground Space Technology, 80*, 53–63.
Ng, C. W. W., Hong, Y., & Soomro, M. A. (2015). Effects of piggyback twin tunnelling on a pile group: 3D centrifuge tests and numerical modelling. *Géotechnique, 65*(1), 38–51.
Ng, C. W. W., Liu, G., & Li, Q. (2013a). Investigation of the long-term tunnel settlement mechanisms of the first metro line in Shanghai. *Canadian Geotechnical Journal, 50*(6), 674–684.
Ng, C. W. W., Lu, H., & Peng, S. (2013b). Three-dimensional centrifuge modelling of the effects of twin tunnelling on an existing pile. *Tunnelling and Underground Space Technology, 35*, 189–199.
Pang, C.H. (2006). *The effects of tunnel construction on nearby pile foundation* [Doctoral dissertation, National University of Singapore].
Randolph, M. F. (2003). Science and empiricism in pile foundation design. *Géotechnique, 53*(10), 847–875.
Selemetas, D. (2006). *Response of full-scale piles and piled structures to tunnelling* [Doctoral dissertation, Univeristy of Cambridge].
Selemetas, D., & Standing, J. (2018). Response of full-scale piles to EPBM tunnelling in London Clay. In *Tunnelling in the Urban Environment: Géotechnique Symposium in Print 2017* (pp. 123–136). ICE Publishing.
Shirlaw, J. (1995). Observed and calculated pore pressures and deformations induced by an earth balance shield: Discussion. *Canadian Geotechnical Journal, 32*(1), 181–189.
Soomro, M. A. (2021). 3D finite element analysis of effects of twin stacked tunnels at different depths and with different construction sequence on a piled raft. *Tunnelling and Underground Space Technology, 109*, 103759.
Soomro, M. A., Hong, Y., Ng, C. W. W., Lu, H., & Peng, S. (2015). Load transfer mechanism in pile group due to single tunnel advancement in stiff clay. *Tunnelling and Underground Space Technology, 45*, 63–72.
Soomro, M. A., Kumar, M., Mangi, N., Mangnejo, D. A., & Cu, Z. D. (2022). Parametric study of twin tunneling effects on piled foundations in stiff clay: 3D finite-element approach. *International Journal of Geomechanics, 22*(6), 04022079.
Soomro, M. A., Kumar, M., Xiong, H., Mangnejo, D. A., & Mangi, N. (2020). Investigation of effects of different construction sequences on settlement and load transfer mechanism of single pile due to twin stacked tunnelling. *Tunnelling and Underground Space Technology, 96*, 103171.
Soomro, M. A., Ng, C. W. W., Liu, K., & Memon, N. A. (2017). Pile responses to side-by-side twin tunnelling in stiff clay: Effects of different tunnel depths relative to pile. *Computers and Geotechnics, 84*, 101–116.
Soomro, M. A., Ng, C. W. W., Memon, N. A., & Bhanbhro, R. (2018). Lateral behaviour of a pile group due to side-by-side twin tunnelling in dry sand: 3D centrifuge tests and numerical modelling. *Computers and Geotechnics, 101*, 48–64.
Sun, W., Lin, E., Yang, Z., Ni, P., & Chen, Y. (2024). Damage analysis of buried pipelines subjected to side-by-side twin tunneling based on centrifuge and numerical modeling. *Tunnelling and Underground Space Technology, 146*, 105647.
Zheng, G., Fan, Q., Zhang, T., & Zhang, Q. (2022). Numerical study of the Soil-Tunnel and Tunnel-Tunnel interactions of EPBM overlapping tunnels constructed in soft ground. *Tunnelling and Underground Space Technology, 124*, 104490.
Zheng, G., Lu, P., & Diao, Y. (2015a). Advance speed-based parametric study of greenfield deformation induced by EPBM tunneling in soft ground. *Computers and Geotechnics, 65*, 220–232.
Zheng, G., Wang, R., Lei, H., Zhang, T., & Fan, Q. (2023). Load-transfer-associated settlements of a piled building during shield tunnelling in soft ground. *Tunnelling and Underground Space Technology, 133*, 104964.
Zheng, G., Zhang, T., & Diao, Y. (2015b). Mechanism and countermeasures of preceding tunnel distortion induced by succeeding EPBS tunnelling in close proximity. *Computers and Geotechnics, 66*, 53–65.